ZC3HC1 is a structural element of the nuclear basket effecting interlinkage of TPR polypeptides

Philip Gunkel and Volker C. Cordes*
Max Planck Institute for Multidisciplinary Sciences, 37077 Göttingen, Germany

ABSTRACT **The nuclear basket (NB), anchored to the nuclear pore complex (NPC), is commonly looked upon as a structure built solely of protein TPR polypeptides, the latter thus regarded as the NB's only scaffold-forming components. In the current study, we report ZC3HC1 as a second structural element of the NB. Recently described as an NB-appended protein omnipresent in vertebrates, we now show that ZC3HC1, both in vivo and in vitro, enables in a stepwise manner the recruitment of TPR subpopulations to the NB and their linkage to already NPC-anchored TPR polypeptides. We further demonstrate that the degron-mediated rapid elimination of ZC3HC1 results in the prompt detachment of the ZC3HC1-appended TPR polypeptides from the NB and their release into the nucleoplasm, underscoring the role of ZC3HC1 as a natural structural element of the NB. Finally, we show that ZC3HC1 can keep TPR polypeptides positioned and linked to each other even at sites remote from the NB, in line with ZC3HC1 functioning as a protein connecting TPR polypeptides.**

Monitoring Editor
Karsten Weis
ETH Zurich

Received: Feb 8, 2022
Revised: May 12, 2022
Accepted: May 17, 2022

INTRODUCTION

The nuclear basket (NB) is a delicate fibrillar structure of eightfold-rotational symmetry that occurs attached to the nuclear side of the nuclear pore complex (NPC). The NB is common to many eukaryotes, and it might be present in almost all vertebrate cell types. The prototypic version of this structure is composed of rectilinear fibrils that emanate from the NPC's nuclear ring (NR), bifurcate at their distal ends, and laterally interconnect with their neighboring fibrils, thereby forming an arrangement referred to as the NB's terminal ring. A range of diverse functions has been ascribed to the NB and some of its attributed components in different cell types and species. Among such functions are roles in perinuclear chromatin organization, gene expression regulation, and nucleocytoplasmic transport (e.g., Krull *et al.*, 2010; Strambio-De-Castillia *et al.*, 2010; Niepel *et al.*, 2013; Snow and Paschal, 2014; Aksenova *et al.*, 2020; Ashkenazy-Titelman *et al.*, 2020; Bensidoun *et al.*, 2021). However, it remains to be unveiled which universal, cell type–spanning function this structure might have.

The NB scaffold in vertebrates comprises numerous copies of a protein called TPR (e.g., Cordes *et al.*, 1997; Frosst *et al.*, 2002; Krull *et al.*, 2004). This large protein features a long, coiled-coil–dominated amino-terminal domain that forms rod-like fibrils and an additional carboxy-terminal domain that, for the most part, is intrinsically disordered and thus considered highly flexible (e.g., Mitchell and Cooper, 1992; Hase *et al.*, 2001). Vertebrate TPR and its homologues in other phyla are commonly looked upon as the only scaffold-forming elements of these organisms' NBs, to which several additional NB-resident proteins merely attach. Among these are, in vertebrates, the SUMO protease SENP1 (e.g., Schweizer *et al.*, 2013; Duheron *et al.*, 2017), the cell cycle checkpoint regulators MAD1 and MAD2 (e.g., Lee *et al.*, 2008; Schweizer *et al.*, 2013), the

This article was published online ahead of print in MBoC in Press (http://www.molbiolcell.org/cgi/doi/10.1091/mbc.E22-02-0037) on May 24, 2022.

Conflict of interest: The authors declare no conflict of interest.

Author contributions: Conceptualization, V.C.C. and P. G.; data curation, P. G. and V.C.C.; formal analysis, P. G. and V.C.C.; investigation, P. G. and V.C.C.; methodology, P.G. and V.C.C.; project administration, V.C.C. and P. G.; resources, V.C.C.; supervision, V.C.C.; validation, P. G. and V.C.C.; visualization, P. G. and V.C.C.; writing–original draft preparation, V.C.C. and P. G.; writing—review and editing, V.C.C. and P. G. Both authors have read and agreed to the published version of the manuscript.

*Address correspondence to: Volker C. Cordes (Volker.Cordes@mpinat.mpg.de).

Abbreviations used: aa, amino acid(s); AID, auxin-inducible degron; CRISPR/Cas9, Clustered Regularly Interspaced Short Palindromic Repeats/CRISPR-associated protein 9; FA, formaldehyde; IB, immunoblotting; IFM, immunofluorescence microscopy; KD, knockdown; KO, knockout; LNN, lamina-NPC-NB; MCL, master cell line; NB, nuclear basket; NB-s, NB-stabilizing; NE, nuclear envelope; NPC, nuclear pore complex; NR, nuclear ring; NUP, nucleoporin; sdAb, single-domain antibody; sfGFP, superfolder green fluorescent protein; T1, TPR pool 1; T2, TPR pool 2.; WT, wild-type.

components of the mRNA export complex TREX-2 (e.g., Umlauf *et al.*, 2013; Wickramasinghe *et al.*, 2014; Aksenova *et al.*, 2020), and the ubiquitin E3 ligase COP1/RFWD2 (Yi *et al.*, 2006; Ouyang *et al.*, 2020). These NB-appended proteins are considered neither structural elements of the NB nor required for NB assembly. Instead, they might use the TPR scaffold as either an operational platform for performing their respective functions or a storage place from which they can be recruited to other subcellular locations upon demand.

Recently, protein ZC3HC1 was presented as another TPR-interacting component of the NB, located at the terminal ring of the NB structure. Although ZC3HC1 is not an essential protein, it likely occurs within most, if not all, vertebrate cell types of different morphogenetic origins in which TPR is also present (Gunkel *et al.*, 2021). In the past, ZC3HC1 had also been described as a nuclear protein with other functions and as engaging in interactions with other proteins that are part of neither the NPC nor the NB (e.g., Ouyang *et al.*, 2003; Bassermann *et al.*, 2005, 2007; Klitzing *et al.*, 2011; Illert *et al.*, 2012; Gengenbacher *et al.*, 2019). Recently, however, ZC3HC1 was shown to not interact naturally with such proteins and instead to be located nearly exclusively at the NB in all of several different cell types investigated (Gunkel *et al.*, 2021).

Furthermore, in contrast to the other NB-resident proteins, ZC3HC1 deficiency was found to cause a substantial proportion of TPR's normally NB-associated amounts no longer to be present there. Instead, such TPR polypeptides remained soluble or were no longer detectable when ZC3HC1 was absent (Gunkel *et al.*, 2021). Inspection of different cell lines further revealed that their NPC-associated amounts of TPR consisted of at least two, then similarly large subpopulations, with one located at the NPC independent of ZC3HC1 and the other requiring the presence of this protein. However, it remained unexplained how ZC3HC1 would contribute to the TPR polypeptides' positioning at the NB and whether it was thereby involved in some direct manner or only indirectly.

In the current study, we now present ZC3HC1 as an unanticipated novel and second structural component of the NB. We demonstrate that ZC3HC1 functions as a connecting element directly required to establish stable interconnections between the subpopulations of TPR at the NB and then maintain the integrity of such higher-order TPR arrangements, at both the NB and sites beyond.

RESULTS

Recently, we found that the knockdown (KD) of *ZC3HC1* transcripts by RNA interference (RNAi) or the disruption of all *ZC3HC1* alleles by CRISPR/Cas9n technology had caused substantial amounts of the NB's scaffold protein TPR to no longer be positioned at the NB (Gunkel *et al.*, 2021). However, it remained unknown whether these findings reflected a direct or indirect role of ZC3HC1, related to either the initial recruitment or adhering of distinct TPR subpopulations to the NB or the subsequent stabilization of their interactions at this site. The current study aimed to unravel which role ZC3HC1 plays in the NB positioning of such additional TPR polypeptides. We will sometimes refer to those anchored at the NPC in a ZC3HC1-independent manner as the TPR pool 1 (T1) polypeptides and to those located at the NE only in the presence of ZC3HC1 as the TPR polypeptides of pool 2 (T2).

ZC3HC1 in vivo is directly involved in the attraction of soluble TPR polypeptides that can be additionally appended to already-NPC-anchored TPR

To gain insight into the course of events leading to the joint residency of ZC3HC1 and the T2 pool at the NB, we determined whether ZC3HC1 can promote the T2 polypeptides' recruitment to this site. To this end, we first investigated whether the conspicuous nuclear amounts of soluble TPR present in some ZC3HC1 knockout (KO) cell lines could be attached to the NE in vivo if one provided sufficiently large amounts of newly synthesized ZC3HC1. Ideally, such amounts would come from induced ectopic expression of ZC3HC1 so fast that substantial amounts of TPR would not be newly synthesized within the same short time. This would ensure that primarily the already existing soluble T2 polypeptides would be available as potential binding partners for the newly appearing ZC3HC1 polypeptides (for further considerations, see Supplemental Information 1).

For these experiments, we used HeLa and HCT116 ZC3HC1 KO cell lines (Gunkel *et al.*, 2021) in which we then had tagged all *TPR* alleles with superfolder GFP (sfGFP; Pédelacq *et al.*, 2006) and in which a conspicuous nuclear pool of soluble sfGFP-tagged TPR was present (Supplemental Figures S1 and S2; Supplemental Information 2; our unpublished data). The representative data presented in Figure 1 stem from the TPR-sfGFP–expressing HeLa ZC3HC1 KO cell line.

To allow for the induced ectopic expression of ZC3HC1, using for this purpose the Tet-On system (Gossen and Bujard, 1992; Gossen *et al.*, 1995), we cloned two ORFs encoding different versions of ZC3HC1 separately into a bidirectional mammalian expression vector derived from the pTetOne expression vector (Heinz *et al.*, 2011; Supplemental Figure S3). This setup allowed for constitutive expression of the Tet-On 3G transactivator and the doxycycline-inducible expression of the two ZC3HC1 versions, which were tagged with mCherry to allow for live-cell imaging. One of the expression vectors encoded the intact wild-type (WT) version of ZC3HC1, and the other would express a ZC3HC1 mutant carrying a single amino acid (aa) substitution (C429S) that abolishes its interaction with TPR (Supplemental Figure S4).

Next, we cell cycle–synchronized the KO cells and transiently transfected them with the plasmids in G2 to allow for nuclear uptake of the vector primarily during postmitotic nuclear reassembly and commencement of the transactivator's constitutive expression from early in G1 onward. The addition of doxycycline, which enabled the transactivator to initiate transcription of the *ZC3HC1* transgenes, followed later in interphase (Figure 1A). From then on, the fate of the nuclear pool of TPR-sfGFP, in the presence of then steadily increasing amounts of mCherry-ZC3HC1, was analyzed by fluorescence microscopy of live cells at different time points (Figure 1, B and C).

We found that the nucleoplasmic pool of TPR remained unaffected in cells transfected with either the "empty" expression vector (our unpublished data) or the vector encoding the NE-binding–incompetent mutant of ZC3HC1, with this holding for all time points investigated. Even in cells with conspicuous amounts of the C429S mutant, there was no increase in TPR signal intensities at their NEs (Figure 1B).

By contrast, in those cells expressing the intact ZC3HC1, we found the gradually intensifying appearance of mCherry-ZC3HC1 at the KO cells' NE to come along with a concomitant increase in the NE-associated TPR signal intensities. The latter was accompanied by a seemingly steady diminishment of the nucleoplasmic TPR pool, with such soluble TPR eventually no longer visible (Figure 1C). Furthermore, in many transfected cells, essentially all of these T2 polypeptides were found attached to the NE already as early as about 30 min to less than 1 h after doxycycline had been added. Thus, in some instances, this was faster than the time required in eukaryotic cells for completing the multistep maturation process

that turns a newly synthesized mCherry polypeptide into a fluorescent protein (Merzlyak *et al.*, 2007; Khmelinskii *et al.*, 2012). Moreover, we estimated that during this short time span between induction of ZC3HC1 synthesis and image acquisition, only 2.5–5% of the cells' total amount of TPR would have been newly synthesized (Supplemental Information 3). The latter meant that most TPR polypeptides recruited back to the NE were indeed those that had already been present as soluble proteins before the synthesis of the new ZC3HC1 polypeptides.

We repeated these experiments with the TPR-sfGFP–expressing HCT116 ZC3HC1 KO cell line, which yielded essentially identical results. Specifically, all of the initially soluble T2 polypeptides were recruited back to the NEs shortly after the induction of WT ZC3HC1 expression, while in cells expressing the C429S mutant, such nucleoplasmic TPR remained soluble (our unpublished data).

Given that expression vectors often end up within a transfected cell's nucleus in high numbers (Cohen *et al.*, 2009; Glover *et al.*, 2010), rapid synthesis of high amounts of ZC3HC1 was not unrealistic, with imaginable theoretical ZC3HC1 copy numbers exceeding those of the T2 polypeptides already after a short time (Supplemental Information 3). Still, we could not yet tell whether the depletion of a nuclear pool of soluble TPR and its reattachment to the NE had been paralleled by ZC3HC1 attachment to the same NEs in amounts proportional to those of TPR. In other words, it remained to be determined whether the NE binding of soluble TPR-sfGFP and mCherry-ZC3HC1 could eventually reach a state in which both proteins' total amounts at the ZC3HC1 KO cells' NEs would be similar to those at the NEs of the WT cells, which would point at similar copy number relationships.

To address this question, we repeated the experiments described in Figure 1, A and C, yet this time started with a cell population composed of the TPR-sfGFP–expressing HeLa ZC3HC1 KO cells and HeLa WT cells naturally expressing the nontagged TPR and nontagged ZC3HC1 polypeptides. This mixed population was then transfected with the expression vector encoding mCherry-ZC3HC1. Because the cells were never all transfected, this allowed for directly comparing the endogenous ZC3HC1 amounts at the NEs of nontransfected WT cells with those of mCherry-ZC3HC1 at the NEs of transfected ZC3HC1 KO cells in which all nuclear TPR-sfGFP had been reattached to the NE. For this purpose, the cells were immunolabeled with ZC3HC1 antibodies and with mCherry-specific single-domain antibodies (sdAbs) to enable detection of the ectopically expressed ZC3HC1 polypeptides with mature and still immature, nonfluorescent mCherry tags. Consequently, the use of such sdAbs, in combination with the KO cells being identifiable via their GFP-tagged TPR polypeptides, allowed for better identification of a transfected KO cell and distinguishing it from both nontransfected and transfected WT cells.

We found that in the transfected KO cells, in which the preexisting nuclear pool of sfGFP-TPR had been gradually and then quantitatively reattached to the NE, the NE-associated amounts of mCherry-ZC3HC1 had risen concomitantly too. Moreover, in some of the transfected KO cells, the amounts of sfGFP-TPR eventually located at the NE appeared to have doubled (Figure 1D). These KO cells likely represented those in which the initially soluble pool, and thus the total amount of TPR, had been larger than the population's mean cellular amount. Notably, such quantitative rerecruitment of soluble sfGFP-TPR to the NE had been accompanied by the NE association of mCherry-ZC3HC1 in amounts that eventually appeared indistinguishable from the amounts of nontagged ZC3HC1 present at the NEs of the nontransfected WT cells (Figure 1D).

One can summarize the conclusions from these in vivo rerecruitment experiments as follows. First, the actual rerecruitment of the soluble TPR polypeptides occurred seemingly proportional to the NE association of the mCherry-ZC3HC1 polypeptides. Eventually, this resulted in some cells being in a steady state in which relative and absolute copy numbers of both proteins at the KO cell's NE were similar to those of the endogenous proteins in the WT cell. Second, we could now essentially rule out a scenario in which the ZC3HC1-dependent attachment of T2 polypeptides to the NPC-anchored TPR pool 1 would be possible only during the formation of entirely new NBs, with the latter impossibly assembled in large numbers in only 30–60 min. Along the same line, it was now clear that the NE appendage of the ZC3HC1-dependent T2 polypeptides could be temporally uncoupled from the ZC3HC1-independent NPC association of TPR pool 1. And finally, these findings meant that the synthesis of ZC3HC1 and TPR polypeptides does not need to happen simultaneously and that potential early interactions between ZC3HC1 and TPR in the cytoplasm are not a prerequisite for later appendage to the NB.

Thus far, we considered it proven that ZC3HC1 polypeptides are directly involved in a process in which TPR polypeptides are recruited from a soluble nuclear pool and appended to those T1 polypeptides already anchored at the NPCs. However, it was still unknown whether the localization of ZC3HC1 at the NB was due to a direct interaction first with the T1 polypeptides, followed by the recruitment of the second TPR pool, or whether ZC3HC1 was merely co-recruited together with the T2 polypeptides. In the latter case, one could imagine that only the binding to T2 polypeptides would allow ZC3HC1, once it had entered the nucleus, to adopt a conformation that would enable it to bind to T1 polypeptides. Alternatively, one could also not yet exclude a scenario in which only the binding to a ZC3HC1 polypeptide in solution would allow the T2 polypeptides to adopt and maintain some distinct conformation that would render them capable of interacting with T1 polypeptides. Thus, while we knew that soluble forms of ZC3HC1 and TPR could, in principle, be coimmunoprecipitated (Gunkel *et al.*, 2021), we could not tell whether such an interaction in solution would be a prerequisite for the two proteins' subsequent binding to the NB. In other words, we did not yet know whether ZC3HC1 and the T2 polypeptides would need to bind concomitantly to the NB or whether such binding could also happen in a stepwise manner.

ZC3HC1 first bound to the NPC-anchored TPR pool 1 in vitro allows for subsequent attraction and appendage of additional TPR pool 2 polypeptides

Studying how ZC3HC1 contributes to the approximate doubling of the NE-associated TPR amounts thus came along with the following questions: Can ZC3HC1 bind directly to the already NPC-anchored TPR pool 1 independently of and thus uncoupled from binding to the T2 polypeptides? And, if so, would the ZC3HC1 polypeptides, once bound to the NB's TPR pool 1, allow for the attraction of additional TPR polypeptides from a soluble pool, as one might then expect?

To address these questions, we established the following experimental setup. HeLa ZC3HC1 KO cells expressing nontagged native TPR were grown in slide wells commonly used for live-cell imaging, to which they tightly adhered during all subsequent treatments. These cells were detergent permeabilized and then washed to remove all traces of soluble T2 polypeptides. The resulting NPC-lamina scaffolds of the NEs (Figure 2A1 and Supplemental Figure S5A), devoid of ZC3HC1 and TPR pool 2 but possessing the NPC-associated TPR pool 1, were then used as assembly platforms, with the latter exhibiting only minor residual autofluorescence in the

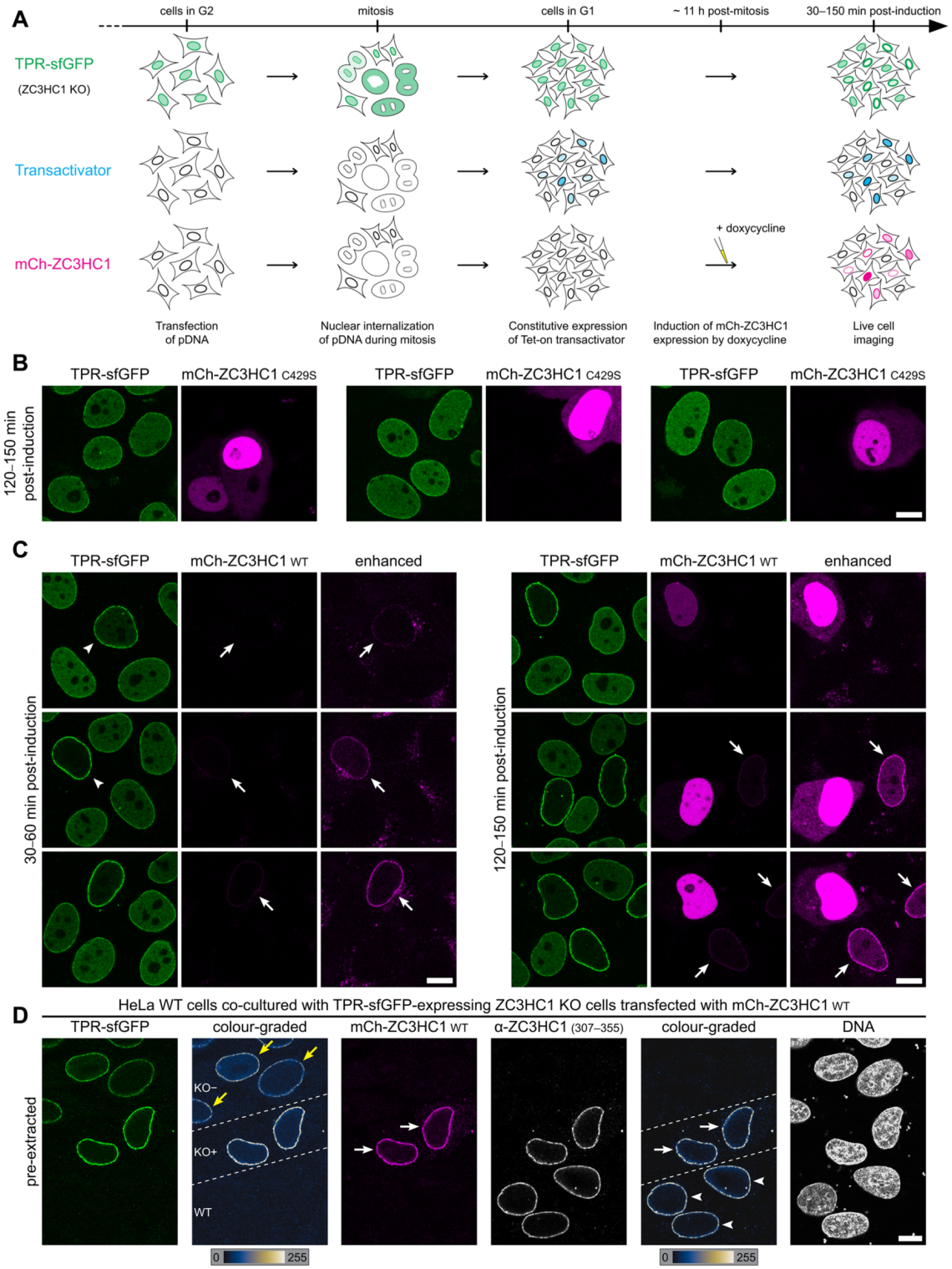

FIGURE 1: Ectopically expressed ZC3HC1 depletes the nuclear pool of soluble TPR in ZC3HC1 KO cells by enabling its recruitment to the NE. (A) Timeline displaying the chronological order of procedures in this experiment schematically. Note that after transfection in G2, the all-in-one vectors encoding the constitutively expressed transactivator and either a doxycycline-inducible WT or mutant version of mCherry-tagged *Hs*ZC3HC1 (see also Supplemental Figure S3) were considered incorporated into nuclei mostly during nuclear reassembly later in mitosis. Constitutive expression and gradual accumulation of the Tet-On transactivator were then directly from the G1 phase on, which allowed for inducing the actual reporter gene expression (here, the WT version depicted) by adding doxycycline at about 11 h postmitosis. (B) Live-cell fluorescence microscopy of TPR-sfGFP–expressing HeLa ZC3HC1 KO cells transfected with an all-in-one vector encoding the mutant version C429S of ZC3HC1, inspected 120–150 min postinduction with doxycycline. The exemplifying micrographs show a selection of transfected cells in which the amounts of the ectopically expressed mutant protein differ. Note that even upon conspicuous expression of this TPR-binding–incompetent mutant, the

520–530 nm wavelength range and essentially none between 540 and 590 nm.

Onto such platforms, we would add mCherry-tagged versions of ZC3HC1, with the one representing the intact protein and the other, again as a control, the C429S mutant incapable of TPR interaction. These two ZC3HC1 variants had been ectopically expressed in HEK293T cells, and from these, we prepared cell extracts that were essentially free of TPR, while each contained one of the two ZC3HC1 variants (Figure 2A2). To this end, we applied a relatively gentle extraction procedure, using digitonin in concentrations also allowing for NE perforation, which resulted in releasing large enough amounts of the recombinant ZC3HC1, primarily located within the HEK293T cells' nuclei, together with only minor amounts of soluble TPR (Figure 2B). The latter, usually hardly detectable in the extracts of nontransfected HEK293T cells, likely represented a consequence of ZC3HC1 overexpression (see also Gunkel *et al.*, 2021). However, to fulfill the requirements for this experimental setup and allow it to be sufficiently informative, even these relatively few TPR polypeptides needed to be removed quantitatively by immunodepletion (Figure 2B). Furthermore, bearing in mind that the concentrations of the mCherry-tagged WT and C429S mutant proteins differed to some extent within the final cell extracts, we determined that their concentrations exceeded those of minor amounts of also present soluble endogenous ZC3HC1 (Supplemental Figure S5, B and C; for approximations of intracellular concentrations, also see Supplemental Information 4). Finally, after adding the TPR-free extracts to the slide wells with the NE scaffolds lacking endogenous ZC3HC1 and thus devoid of all ZC3HC1-dependent TPR, the specimens were immediately inspected by fluorescence microscopy and then further monitored for a certain period of time.

The addition of those extracts containing the ZC3HC1 mutant C429S did not lead to enriched mCherry fluorescence specifically at the NE scaffolds within a predefined time span (Figure 2C). Nonspecific binding to various subcellular structures, never observed with mCherry-tagged WT ZC3HC1, was seen only after prolonged incubation (our unpublished data, but also see Supplemental Information 4). By striking contrast, within seconds after adding the WT version of ZC3HC1, we noted mCherry fluorescence specifically accumulating at the NEs. After a few minutes, this NE-associated fluorescence reached a seemingly constant brightness, indicative of a steady-state level of interactions between the ZC3HC1 polypeptides and some definite number of ZC3HC1 binding sites provided by the T1 polypeptides (Figure 2D). Moreover, while the extracts for the experiments shown here had been adjusted to contain similar concentrations of the mCherry-tagged WT and C429S mutant version, essentially identical results were also obtained when using these proteins in a range of other concentrations too (our unpublished data).

Furthermore, upon washing these NEs to remove all unbound mCherry fluorescence, using the detergent-free NB-stabilizing (NB-s) buffer here called assembly buffer, the NE-associated mCherry-ZC3HC1 was not similarly removed. This finding too pointed to some ZC3HC1:T1 interactions that could last for some time even when T2 polypeptides were absent (Supplemental Figure S6). However, we also noted that these ZC3HC1 interactions with the NE platforms were not similarly long-lasting for all of the appended mCherry-ZC3HC1 polypeptides. We found some of those initially attached to the NE scaffolds swiftly detaching again when washed in assembly buffer, eventually resulting in only about half of the initially NE-appended amount of ZC3HC1 durably remaining bound

nucleoplasmic pool of TPR-sfGFP remained unaffected, being indistinguishable in appearance from that of neighboring untransfected cells. Bar, 10 µm. (C) ZC3HC1 KO cells like those in B but transfected with an expression vector encoding the mCherry-tagged intact WT version of ZC3HC1 capable of binding to the NE. These cells were inspected either 30–60 min or 120–150 min postinduction. Microscope settings were identical at the different time points, as was the degree of mCherry signal enhancement that was done only after image acquisition. The exemplifying micrographs show a selection of transfected cells with different amounts of the ectopically expressed protein. Note that these images cannot claim to represent a proper time course experiment that allows for correlating timespan with gradual protein accumulation within transfected cells at different time points, simply because plasmid copy numbers per cell likely vary significantly between cells. Nonetheless, already after short time lengths, the nuclear pool of GFP-tagged TPR was notably diminished or no longer detectable (two exemplifying nuclei marked by arrowheads). The latter was even so in those transfected cells (several demarked by arrows) in which the amounts of ZC3HC1 synthesized until then were barely detectable via their mCherry tags at standard microscope settings, likely due to the relatively slow and here not yet completed mCherry maturation, which in turn also prompted the presentation of electronically brightness-enhanced images. Bar, 10 µm. (D) IFM of cell-cycle–synchronized cells transfected with the all-in-one mCherry-ZC3HC1 expression vector and treated with doxycycline as outlined in A, yet having started with a mixed population of TPR-sfGFP–expressing ZC3HC1 KO cells and HeLa WT cells expressing ZC3HC1 and nontagged TPR. Such mixed populations allowed for comparing the amount of endogenous ZC3HC1 at the WT cell's NE relative to that eventually occurring at the ZC3HC1 KO cell's NE, here focusing on those KO cells in which the mCherry signal intensity at the NE seemed to have reached a maximum. Cells shown here were harvested 120 min postinduction and then detergent-permeabilized before fixation. The latter allowed for removing 1) the soluble pool of TPR still existing in the nontransfected KO and 2) the surplus of soluble mCherry-ZC3HC1 for which no further binding sites existed at the NEs of the transfected cells, which, in turn, allowed for a better assessment of signal intensities at only the NEs. The cells were then fixed with FA before being labeled with a *Hs*ZC3HC1 antibody and a sdAb specific for mCherry. Micrographs showing sfGFP-tagged TPR and antibody-labeled ZC3HC1 are also shown colorgraded to display differences in pixel intensities via a color LUT, with areas harboring WT cells, two transfected KO cells (KO+), and some nontransfected KO cells (KO–) marked accordingly. Note that the intensities of ZC3HC1 immunolabeling at the WT cells' NEs (marked by arrowheads in the color-graded micrograph on the right side) and at the NEs of those ZC3HC1 KO cells that had been ectopically expressing mCherry-ZC3HC1 (white arrows) were very similar. As an aside, also note again that TPR signal intensities at the NEs of those KO cells ectopically expressing ZC3HC1 (see KO+ cells in the color-graded micrograph on the left) were notably higher than at the NEs of those neighboring cells on the same coverslip that had remained nontransfected (KO–) and lacked mCherry fluorescence (yellow arrows). Bar, 10 µm.

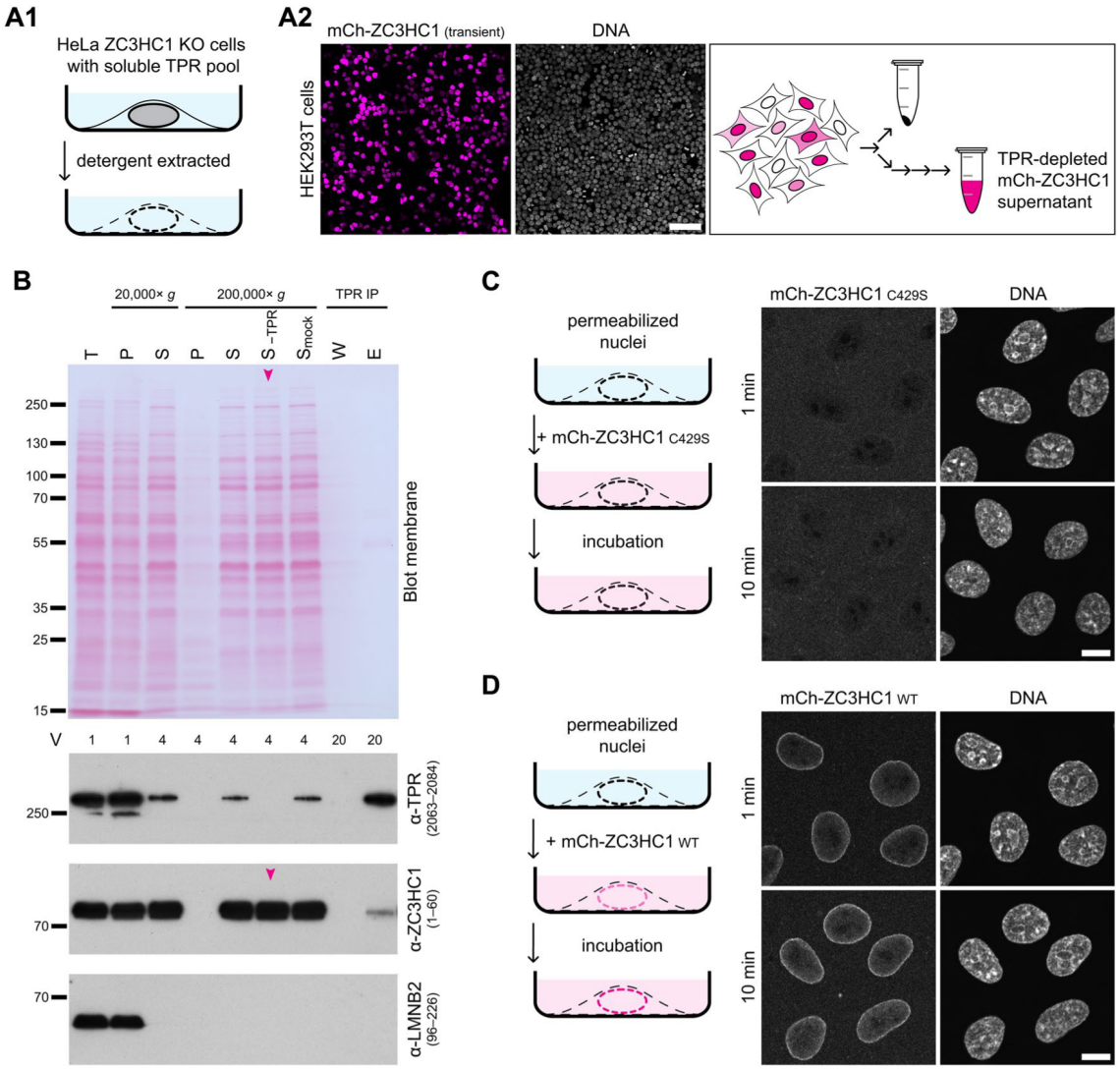

FIGURE 2: Ectopically expressed ZC3HC1 can bind to the ZC3HC1-independent pool of NPC-anchored TPR polypeptides in vitro. (A) Depiction of experimental materials and starting conditions, comprising (A1) HeLa ZC3HC1 KO cells permeabilized with TX-100 and cleared of soluble TPR polypeptides (for additional information, see Supplemental Figure S5), and (A2) supernatants of HEK293T cell extracts containing ectopically expressed variants of mCherry-ZC3HC1. The latter were obtained after cell permeabilization with elevated concentrations of digitonin, high-speed centrifugation, and immunodepletion of TPR. The micrographs in A2 show representative live-cell images of the transiently transfected cell population, also schematically depicted on the right. Bar, 100 µm. (B) IBs of a selection of the cellular fractions obtained from HEK293T cells ectopically expressing mCherry-ZC3HC1. Loaded fractions included the total cell extract (T) and the digitonin-containing soluble cell extracts, obtained after 20,000 and 200,000 × *g* centrifugation and containing minor amounts of soluble TPR (S 20,000 and S 200,000), which was common for HEK293T cells ectopically expressing large amounts of recombinant ZC3HC1. Loadings also included the corresponding pellets of these centrifugation steps (P 20,000 and P 200,000), the 200,000 × *g* cell extract supernatant mock-depleted with magnetic beads only coated with protein A (S_{mock} 200,000) and the same supernatant TPR-depleted with protein A beads coated with *Hs*TPR antibodies (S_{-TPR} 200,000). Such latter supernatant cleared of TPR is here marked with an arrowhead and represented the mCherry-ZC3HC1–containing cell extract eventually used for the interaction experiments. For further comparison, additional lanes were loaded with materials released from the TPR beads during the second of two successive washing steps (W) and those eventually eluted from these beads with SDS-containing sample buffer (E). Most lanes were loaded with the respective amount from the same number of HEK293T cells (4 V), while relative amounts of the total cell extract and the 20,000 × *g* pellet material corresponded only to one fourth thereof (1 V), whereas the W and TPR-IP fractions represented fivefold higher relative amounts (20 V). The incubations with *Hs*TPR and *Hs*ZC3HC1 antibodies and, for comparison, with LMNB antibodies, were on different parts of the Ponceau S–stained membrane shown here and on another one with identical amounts loaded. Note that essentially no TPR was detectable within the 200,000 × *g* supernatant after the TPR depletion procedure. As an aside, also note that the fraction of immunodepleted TPR contained coimmunoprecipitated mCherry-ZC3HC1, which underscored the necessity to remove the minor pool of soluble TPR from the 200,000 × *g* supernatant to avoid the experiment's conclusiveness spoiled by soluble TPR-ZC3HC1 assemblies. (C, D) Fluorescence microscopy of detergent-extracted ZC3HC1 KO cells incubated with TPR-free cell extracts containing similar amounts of either (C) the mCherry-tagged

to the T1 polypeptides (Supplemental Figure S6). Such detachment of a certain amount of mCherry-ZC3HC1 differed from what one could observe with similarly detergent-extracted HeLa WT cells harboring endogenous ZC3HC1 and both pool 1 and pool 2 of TPR. When we kept such detergent-extracted WT cells in the same assembly buffer, the NE association of ZC3HC1, as part of likely more complex assemblies involving ZC3HC1 and both pools of TPR, was not notably affected by similarly long incubations (our unpublished data, but see also further below).

Nonetheless, having demonstrated that ZC3HC1 can bind to the NE independently of the T2 polypeptides, we then asked whether these bound ZC3HC1 polypeptides would allow for the recruitment of additional TPR polypeptides and for keeping them tethered there at the NE. To this end, we prepared cell extracts from sfGFP-TPR–expressing HeLa ZC3HC1 KO cells in which a large proportion of such tagged TPR was occurring throughout the nuclear interior as a soluble pool (Figure 3A and Supplemental Figure S2D). After high-speed centrifugation, such ZC3HC1-deficient extracts were also free of trace amounts of NE fragments (Figure 3B) while containing large amounts of exclusively soluble sfGFP-tagged TPR (see also Supplemental Information 4).

Given that especially GFP fluorescence in cultured cells can be contaminated to some extent by cellular autofluorescence (Niswender *et al.*, 1995), we had first assessed the threshold beyond which one could discriminate GFP signals from autofluorescence. For this purpose, we had inspected the detergent-extracted HeLa ZC3HC1 KO cells, then only in assembly buffer, for the relative levels of residual autofluorescence at different wavelengths. Microscope settings, subsequently chosen for obtaining the experiments' original micrographs, and the degree of subsequent electronic signal enhancement were then kept the same for the corresponding images presented in Figure 3, C and D. With these settings, essentially no autofluorescence was detected in the original micrographs representing the mCherry excitation wavelengths, while some autofluorescence had to be taken into account as background at wavelengths that would excite GFP (Figure 3C).

When we then incubated the NE scaffolds devoid of ZC3HC1 and T2 polypeptides with the sfGFP-tagged TPR polypeptides only, this did not result in any pronounced accumulation specifically at the ZC3HC1-deficient NEs. At some of these NEs, hardly any or no sfGFP fluorescence was detectable at all, while at others, the sfGFP levels were only marginally enhanced relative to the autofluorescence (Figure 3C). Whether this reflected some weakish interactions between the sfGFP-tagged TPR polypeptides and other NE proteins, or perhaps even some weak direct interactions between the different TPR populations, could not be resolved in the current study.

Clearly, however, when the NE scaffolds had already been loaded with mCherry-ZC3HC1, meaning that such ZC3HC1 had first been allowed to interact with the available TPR pool 1 binding sites, followed by removing the nonbound ZC3HC1 surplus and briefly washing these NE scaffolds, and only then incubating them with the sfGFP-tagged TPR polypeptides, we found that the latter markedly accumulated at the NE (Figure 3D; for further details, see Supplemental Information 5).

To assess how lasting and robust these in vitro interactions were, now between ZC3HC1 and both pools of TPR, we again allowed mCherry-ZC3HC1–loaded NE scaffolds to attract steady-state levels of sfGFP-TPR, followed by again washing these NEs with buffer and then keeping them therein for many hours. While they were sometimes moderately reduced after prolonged periods, we recurrently found the NE-associated levels of sfGFP and mCherry fluorescence still prominent. After 10–12 h of incubation in the cell extract–free buffer at room temperature (RT), the washed NE's fluorescence levels were often indistinguishable from those of the same experiment's sfGFP-TPR–loaded NEs directly after extract removal and brief washing (Figure 3E and our unpublished data). This finding suggested that the interplay between ZC3HC1 and the different TPR pools had allowed for a lasting NE positioning of the T2 polypeptides and those ZC3HC1 polypeptides enabling this.

Altogether, we interpreted the in vitro data in such a way that ZC3HC1 polypeptides, once attached to the NPC-appended pool 1 of TPR, allow for the subsequent recruitment of T2 polypeptides and promote interactions with those of pool 1. It was also already tempting to consider ZC3HC1 as a structural element that would either stabilize the interactions between the NB's different TPR populations or even function as a direct interconnector between them. However, at this point, we could not yet draw this conclusion because we could not yet exclude another scenario, which would resemble the relationship between the NPC protein NUP153 and the NPC-anchored TPR pool 1 polypeptides (for further details, see Supplemental Information 6). In this scenario, ZC3HC1 again would enable the establishment of higher-order arrangements between the T1 and T2 populations, reminiscent of the role of NUP153 in enabling arrangements between the T1 polypeptides and other NPC components. However, just as NUP153 appears to be dispensable for the NB's integrity once the T1 polypeptides occur NPC anchored (Supplemental Information 6), ZC3HC1 would no longer be needed to maintain the integrity of NB structures composed of T1 and T2 polypeptides, once these have been assembled. Thus, so long as it remained uncertain whether ZC3HC1 is needed for maintaining the T2 polypeptides' arrangements at the NB, we would not yet declare ZC3HC1 a structural NB element.

ZC3HC1 in vivo is directly required for keeping TPR subpopulations attached durably to those TPR polypeptides that occur NPC anchored independently of ZC3HC1

The uncertainty regarding the potential role of ZC3HC1 as a structural element was also due to the circumstance that formerly

C429S mutant version of ZC3HC1 incapable of TPR binding or (D) the WT ZC3HC1 protein. Interaction experiments were performed in parallel in neighboring wells, and images of the unfixed cells, also stained with the DNA dye Hoechst 33342, were acquired with identical microscope settings at 1 and 10 min after adding the cell extracts. Because of the necessity to omit anti-fade media and the fact that focusing on the equatorial plane of the extracted cells was more time-consuming than for intact or fixed cells, images taken at different time points were not from identical groups of cells but only from neighboring groups of the same sample, to avoid pronounced photobleaching. Moreover, reduced laser power, compared with that for IFM images, was chosen for the image acquisition of the in vitro assembly experiments, which later was followed by electronic brightness enhancement in the same proportional manner and identical extent for all of these images (see *Material and Methods*). Note that no mCherry fluorescence appeared to be enriched specifically at the NEs treated with the C429S mutant. By contrast, those NE scaffolds incubated with the WT version for a similarly long time were notably fluorescent. Bars, 10 µm.

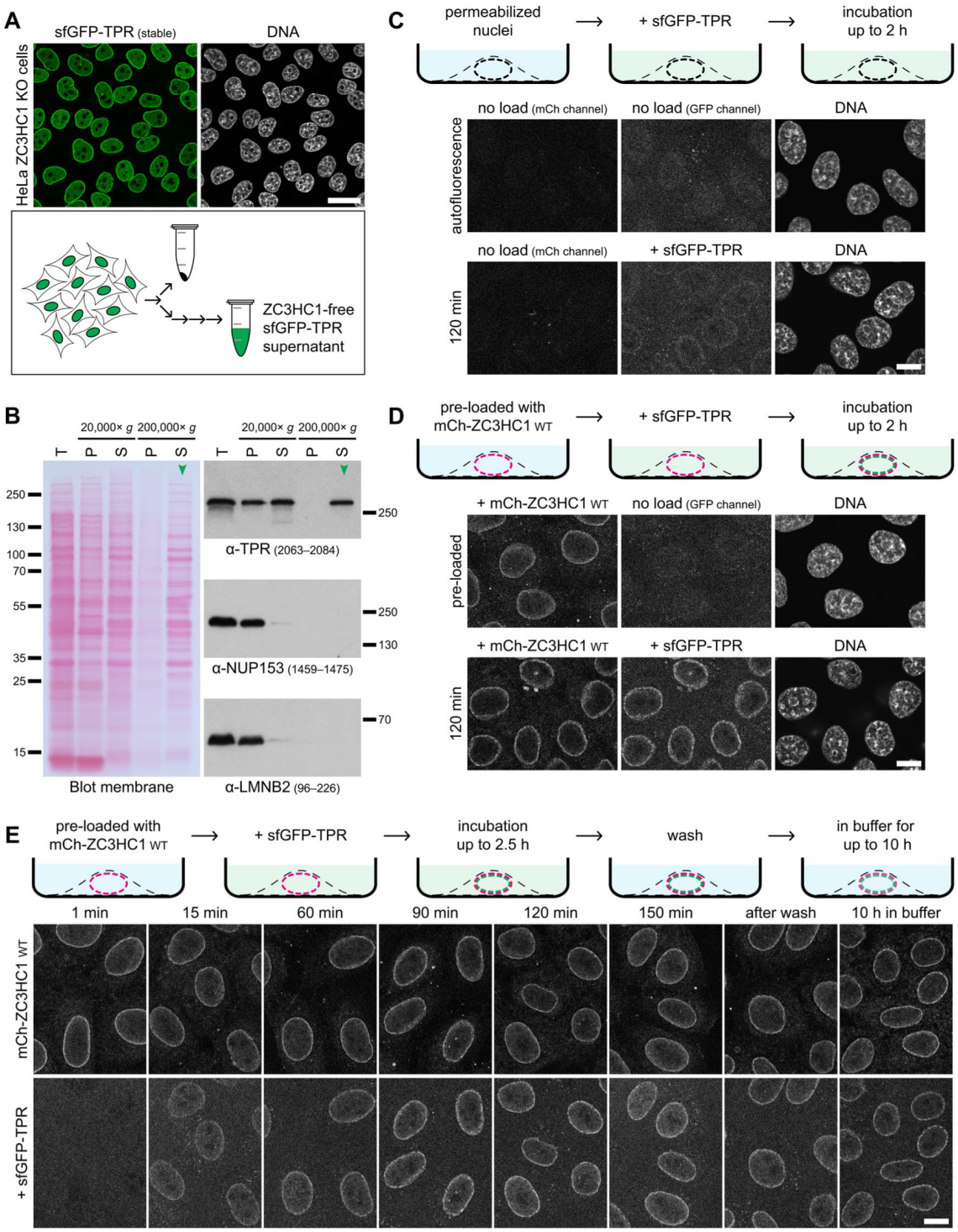

FIGURE 3: Ectopically expressed ZC3HC1 loaded onto the ZC3HC1-independent pool of NPC-anchored TPR can attract additionally provided TPR polypeptides, resulting in both types of proteins steadily appended to the NE. (A) Representative live-cell image of the sfGFP-TPR–expressing HeLa ZC3HC1 KO cell line, next to a schematic depiction of the high-speed supernatant of a detergent-free extract isolated from such cells containing the soluble pool 2 polypeptides of sfGFP-TPR. Bar 25 µm. (B) IBs of a selection of the cellular fractions from the sfGFP-TPR–expressing ZC3HC1 KO cells. Loaded fractions included the total cell extract (T), the soluble extracts obtained after cell disruption by gentle sonication and subsequent centrifugation at 20,000 × *g* (S 20,000) and 200,000 × *g* (S 200,000), and the corresponding pellet fractions (P 20,000 and P 200,000). Lanes were loaded with amounts corresponding to the same number of HeLa ZC3HC1 KO cells. Immunolabelings for TPR, NPC component NUP153, and nuclear lamina component LMNB, the two latter proteins shown for comparison, were on different parts of the Ponceau S–stained membrane shown here and on an identically loaded duplicate. Note that the 200,000 × *g* supernatant, marked with an arrowhead and representing the cell extract with the soluble sfGFP-TPR categorized as pool 2 polypeptides and eventually used for the interaction experiments, was virtually free of LMNB and NUP153. This finding indicated that the solution did not

observed phenotypes, such as the appearance of soluble TPR pools following the destruction of *ZC3HC1* transcripts by RNAi or after CRISPR/Cas9n-mediated disruption of the *ZC3HC1* alleles (Gunkel *et al.*, 2021), had manifested themselves only time delayed. In other words, before RNAi had eventually resulted in notably diminished ZC3HC1 protein amounts or before having accomplished the unavoidably lengthy process of isolating ZC3HC1 KO cell clones, these cells had passed through mitosis. However, because vertebrate NBs are disassembled at the outset of mitosis and need to be postmitotically reassembled again from soluble components, one could then not unambiguously distinguish between a direct or an indirect role for ZC3HC1 in either the recruitment or appendage of the TPR polypeptides or in keeping them bound to the NB. While recruitment and appendage experiments (Figures 1–3) had now allowed for a close spatiotemporal correlation between ZC3HC1 availability and the resulting NB positioning of the T2 polypeptides, we still needed a similarly conclusive direct correlation between induced ZC3HC1 deficiency and the resultant impact on these ZC3HC1-dependent TPR polypeptides once they occurred appended to the NB.

We considered it possible that degron-based technologies could achieve sufficiently rapid ZC3HC1 elimination and allow for the manifestation of phenotypes without cells passing through mitosis. Thus, we created yet further CRISPR/Cas9-edited cell lines, of which one would allow for the inducible degradation of the then degron-tagged ZC3HC1 polypeptides, while the other, for comparison, would similarly permit degrading TPR.

To this end, we constructed an insertion cassette, referred to as sfGFP^{L9mIAA7}, which encoded a double tag comprising an auxin-inducible degron (AID)-tag (Li *et al.*, 2019) and sfGFP. We positioned this AID-tag (mIAA7) within loop 9 of sfGFP, where we had found it fully functional as a degron while only marginally attenuating sfGFP's ability to fluoresce (Supplemental Figure S7A, our unpublished data, and see further below).

In addition, we had integrated another cassette, which allowed for constitutive expression of the *AFB2* (auxin signaling F-box 2 protein) gene from *Arabidopsis thaliana* (Li *et al.*, 2019), into the genome of the HCT116 cell line, which we used from then on as the master cell line (MCL; Supplemental Figure S7, B and C). We chose HCT116 as the first cell line for performing such ZC3HC1 degradation experiments because it is nearly diploid, had been used in the prequel study on ZC3HC1 (Gunkel *et al.*, 2021), and had already been proven suitable for AID tagging and auxin-inducible target degradation (Natsume *et al.*, 2016).

Targeting the *ZC3HC1* and *TPR* alleles in this HCT116 MCL, we isolated homozygous cell lines in which all TPR (Supplemental Figure S8) or all ZC3HC1 polypeptides (Supplemental Figure S9) possessed the sfGFP^{L9mIAA7} tag. Immunofluorescence microscopy (IFM) revealed that the NE-attached amounts of the tagged polypeptides in most cells were seemingly indistinguishable from those of the corresponding tag-free polypeptides at the progenitor cell line's NEs (Figures 4A1 and 5A1), indicating that the tag allowed for largely quantitative NB association of both TPR and ZC3HC1. While we occasionally observed minor differences in the cell populations' total amounts of tagged and nontagged polypeptides when the 5′ end of some genes, including *TPR*, had been tagged, we found such minor variations not to affect the outcome of the here presented degradation experiments.

Next, we triggered TPR degradation in the sfGFP^{L9mIAA7}-TPR cell line by adding auxin, which resulted in essentially all TPR degraded within less than 90 min (Supplemental Figure S10A and further below). In addition, this had come along with ZC3HC1 displaced from the NE and then present only in soluble form within the nucleoplasm (Figure 4, A2 and B). Thus, in line with former TPR RNAi

contain tiny NE and NPC fragments, which one might have expected due to the sonication process. Furthermore, it neither contained considerable amounts of NUP153 as the only other known TPR-binding protein reported to play a role in binding TPR subpopulations to NPCs. (C) Fluorescence microscopy of the detergent-extracted ZC3HC1 KO cells in the complete absence of ZC3HC1, both before (no load) and after incubation with the ZC3HC1-free but sfGFP-TPR–containing cell extract at RT (120 min). Note that the images of the not-loaded cells labeled "mCh channel" and "GFP channel" actually reflected the degree of autofluorescence of detergent-extracted HeLa cells at different wavelengths. With the microscope settings chosen, essentially no autofluorescence was detected at the mCherry excitation wavelengths, while only some autofluorescence was notable at wavelengths that would excite GFP. These microscope settings were kept the same also for corresponding images in D and E. Further note that after incubations of up to 120 min with the sfGFP-TPR extract, there was hardly any sfGFP fluorescence detected at some of the ZC3HC1-deficient NEs, while it was only marginally enhanced at others beyond the autofluorescence background in this wavelength range. Bar, 10 µm. (D) Fluorescence microscopy, with microscope settings as in C, but here of NE scaffolds that had first been loaded with the mCherry-tagged WT version of *Hs*ZC3HC1, followed by the removal of the unbound surplus of mCherry-ZC3HC1 by brief washes with assembly buffer (preloaded specimen). Soluble sfGFP-TPR polypeptides were added immediately after the last wash, using the same sfGFP-TPR aliquot as for C, with interaction experiments shown as C and D performed almost simultaneously in parallel in neighboring wells, with the double-loaded specimens shown here also imaged after 120 min. Note that the sfGFP-tagged TPR polypeptides had specifically and conspicuously accumulated at the NE scaffolds preloaded with mCherry-ZC3HC1. As an aside, one needs to mention that sfGFP-TPR signal intensities at the NEs of the permeabilized cells would not have been able to reach the levels in a WT cell expressing all pool 1 and pool 2 TPR polypeptides as tagged with sfGFP, because all pool 1 TPR polypeptides within the ZC3HC1 KO cells, here used as binding platforms, were untagged. Bar, 10 µm. (E) Fluorescence microscopy of initially ZC3HC1-deficient NE scaffolds that had been loaded with mCherry-ZC3HC1 first, then briefly washed in assembly buffer, immediately incubated in an sfGFP-TPR–containing cell extract for 150 min, washed again, and then kept within the same assembly buffer for at least 10 h. In this experiment, distinct from the one in D, the specimens were inspected at different time points, revealing gradual accumulation of the sfGFP-TPR polypeptides at the mCherry-ZC3HC1–loaded NEs until seemingly reaching a steady-state level of TPR at such NEs. Note that this binding appeared rather persistent following the extract removal and brief washing ("after wash"), with only moderate reduction of the NE-associated sfGFP and mCherry fluorescence even after prolonged incubation in cell extract–free buffer at RT overnight. Bar, 10 µm.

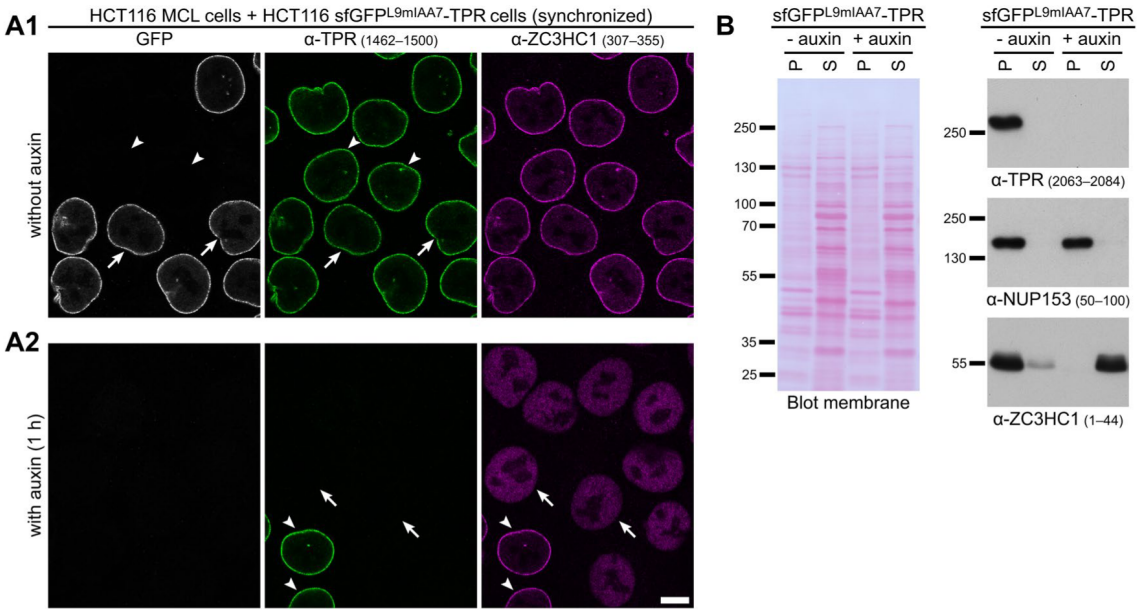

FIGURE 4: Auxin-induced TPR degradation in a homozygous sfGFP^{L9mIAA7}-TPR cell line results in the detachment and solubilization of NB-bound ZC3HC1. (A) IFM of cells from the HCT116 progenitor MCL expressing the naturally tag-free TPR and cells of the homozygous HCT116 progeny line, in which all TPR polypeptides occur N-terminally tagged with sfGFP^{L9mIAA7}. Cells had been cocultured and synchronized as mixed populations together on the same coverslip, followed by an additional incubation of 1 h in the absence (A1) or presence (A2) of auxin. Specimens were then double-immunolabeled for TPR and ZC3HC1 and analyzed in parallel, using identical microscope settings. Arrowheads mark the nuclei of some MCL cells, i.e., those expressing the tag-free version of TPR, while arrows point at some of the progeny cells' nuclei, i.e., those with the sfGFP-tagged TPR. Note, in A1, that the amounts of sfGFP^{L9mIAA7}-tagged TPR appended to the NEs did not notably differ from the amounts in the neighboring tag-free cells. Further note, in A2, that auxin treatment resulted in the complete elimination of any visible NE-associated GFP and TPR immunostaining in those cells that had been expressing the tagged version of TPR, while the MCL cells' untagged TPR polypeptides remained unaffected. In particular, note that eliminating the tagged TPR had caused ZC3HC1 to be no longer detectable at the NE but distributed throughout most of the nuclear interior instead. Bar, 10 µm. (B) IB of cell extracts obtained from the sfGFP^{L9mIAA7}-TPR HCT116 cells treated with auxin, or only with DMSO, for 1 h. Similar numbers of cells of the two differently treated batches had then been extracted with TX-100 in parallel, resulting each in a fraction of soluble proteins (S) and a corresponding pellet fraction (P) also containing the NPCs and normally, that is, in the absence of auxin, the complement of NB proteins. Equal portions of each fraction's whole amount were loaded for SDS–PAGE and IB. Incubations with *Hs*TPR and *Hs*ZC3HC1 antibodies, and *Hs*NUP153 antibodies for comparison, were on different parts of the Ponceau S–stained membrane shown here and on another one with identical loadings. Note that TPR was no longer detectable after auxin treatment. Moreover, ZC3HC1, mainly part of the LNN-enriched pellet fraction of cells not treated with auxin, had been released into solution upon auxin-induced TPR degradation, while the exclusive presence of NUP153 within the NPC-NB–enriched fraction had remained unaffected.

experiments indicating that TPR represents the only anchor point for ZC3HC1 at the nuclear periphery (Gunkel *et al.*, 2021), the current result confirmed that all ZC3HC1 polypeptides longer-lastingly positioned at the NE are located there only because of their interactions with TPR.

Of further note, TPR degradation had also resulted in the detachment of other known TPR binding partners from the NE, here exemplified by IFM for MAD1, GANP, and SENP1 (Supplemental Figure S11). Strikingly, though, while the detachment of some NB components, like ZC3HC1, was found to correlate temporally strictly with TPR's degradation, this was not the case for others, here exemplified by GANP. At some early points, when essentially all TPR had already been degraded and virtually all ZC3HC1 had been concomitantly detached from the NE, almost all GANP polypeptides were still occurring NE positioned (Supplemental Figure S12), from where they then only gradually detached over time. Such degron-based investigations thus allowed for assigning the NB-associated proteins to distinct categories, with ZC3HC1 exemplifying those proteins whose NB residency in proliferating culture cells appears to be solely TPR dependent. Others, like GANP, appear to engage in versatile interactions with yet other proteins at the nuclear periphery, with some of the latter on their own capable of keeping an NB-associated protein positioned at the NE for some time. Nonetheless, in the end, all of the proteins so far regarded as ratified NB components, including GANP, had in common that they could not lastingly remain positioned at the NPC when TPR was absent (Supplemental Figure S11; our unpublished data; for further details, also see Supplemental Information 7).

However, the result we regarded as the most informative was obtained after having triggered the degron-mediated degradation of ZC3HC1, which resulted in its essentially complete degradation within 90 min. Most strikingly, such disappearance of ZC3HC1 was accompanied by roughly half the total amount of NE-appended TPR no longer occurring attached to the NE (Figure 5A2). Instead, a conspicuous amount of TPR was then found distributed within the nucleoplasm (Figure 5A2).

The more precise quantification of the residual signal intensities for immunolabeled TPR at the ZC3HC1-deficient NEs revealed a reduction by more than half and sometimes up to about 60% of the total NE-associated TPR amounts present before ZC3HC1

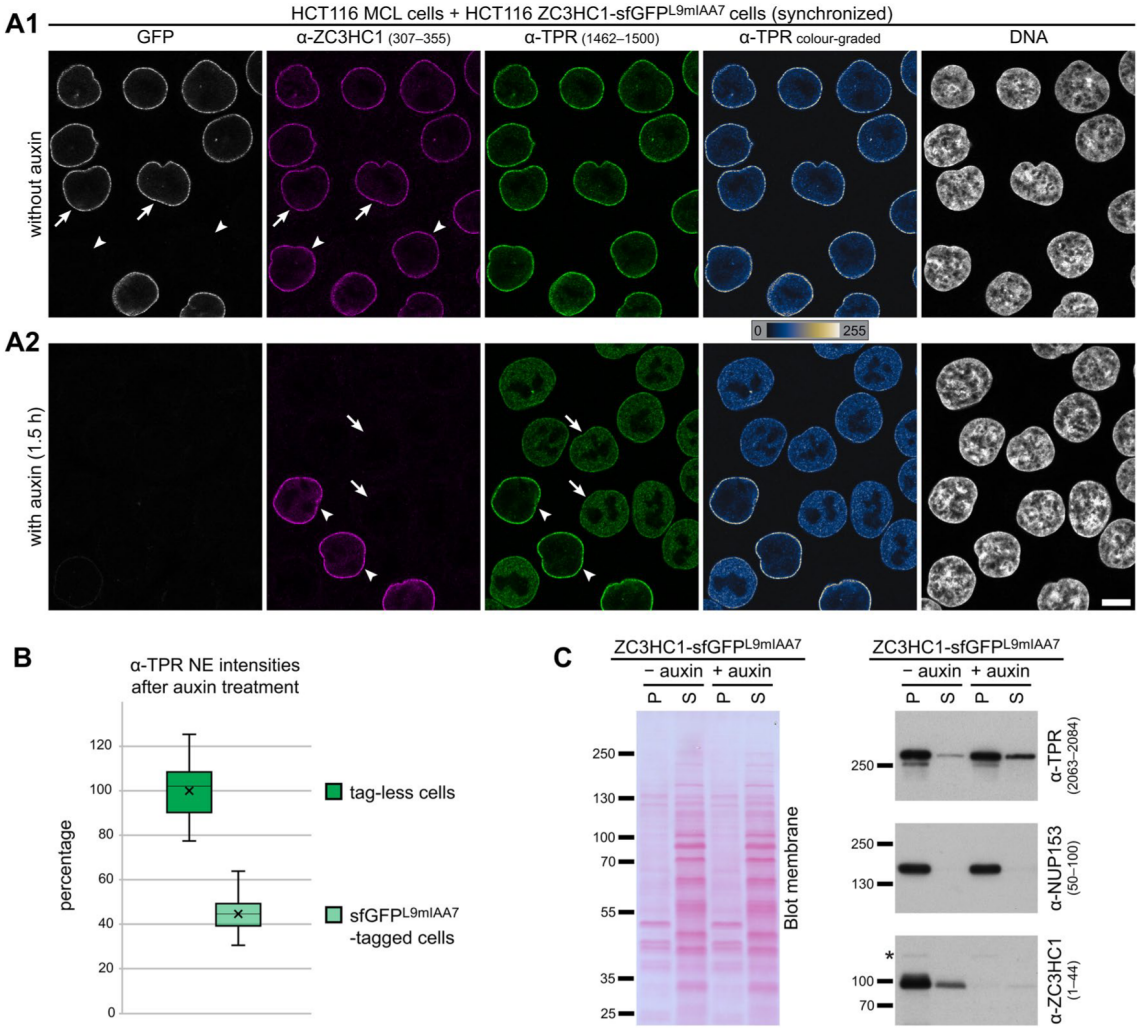

FIGURE 5: Auxin-induced rapid and quantitative ZC3HC1 degradation in a homozygous ZC3HC1-sfGFP^{L9mIAA7} cell line results in the concomitant detachment of large amounts of NB-positioned TPR. (A) IFM of cells from the HCT116 progenitor MCL expressing the naturally tag-free ZC3HC1 and cells of the homozygous HCT116 progeny line, in which all ZC3HC1 polypeptides were C-terminally tagged with sfGFP^{L9mIAA7}. Cells had been cocultured and synchronized as mixed populations together on the same coverslip, followed by an additional incubation of 90 min in the absence (A1) or presence (A2) of auxin. Specimens were then double-immunolabeled for ZC3HC1 and TPR and analyzed in parallel, using identical microscope settings, with staining for TPR also shown color graded to display differences in pixel intensities via a color LUT. Arrowheads mark the nuclei of some MCL cells, i.e., those expressing the tag-free version of ZC3HC1, while arrows point at some of the progeny cells' nuclei, i.e., those with the sfGFP-tagged ZC3HC1. Note, in A1, that the amounts of sfGFP^{L9mIAA7}-tagged ZC3HC1 appended to the NEs did not notably differ from the amounts in the neighboring tag-free cells. Further note, in A2, that auxin treatment resulted in the elimination of NE-associated GFP and immunostaining for ZC3HC1 in those cells that had been expressing the tagged version of ZC3HC1, while the MCL cells' untagged ZC3HC1 remained unaffected. In particular, note that eliminating the tagged ZC3HC1 had caused a conspicuous reduction in the intensity of TPR immunolabeling at the NE, with a significant amount of TPR then distributed throughout most of the nuclear interior. Bar, 10 μm. (B) Quantification of signal yields for immunolabeled TPR at the NEs, following the incubation with auxin of the same mixed population of HCT116 cells expressing the tag-less and the sfGFP^{L9mIAA7}-tagged ZC3HC1. Randomly chosen NE segments for quantifications (sfGFP^{L9mIAA7}-tagged: $n = 97$; tag-less: $n = 50$) via ImageJ were essentially from all labeled cells in equatorial view within several randomly chosen images, all of which were from the same specimen that also provided the micrograph for A2. Box plots display the relative signal intensity values, with the arithmetic means marked by x, with the ones for the cells not treated with auxin set to 100%, and with the SDs provided. Note that the mean TPR signal yield for the KO cells' ZC3HC1-free NEs was only about half the WT cells' corresponding value. (C) IB of cell extracts obtained from ZC3HC1-sfGFP^{L9mIAA7} HCT116 cells treated with DMSO or with auxin for 90 min. Applying conditions maintaining NB integrity, cells had been extracted with TX-100, resulting in fractions of soluble (S) and nonsoluble proteins (P), with equal portions of each fraction's whole amount then loaded for IB. Incubations with *Hs*TPR and *Hs*ZC3HC1 antibodies, and *Hs*NUP153 antibodies for comparison, were on different parts of the Ponceau S–stained membrane shown here and on another one with identical loadings. The asterisk marks a cross-reaction unrelated to ZC3HC1. Note that ZC3HC1 had been largely degraded after the 90-min treatment with auxin, accompanied by a minor increase in the TPR amount detectable within the soluble cell fraction, while the presence of NUP153 within the pellet fraction had remained unaffected.

degradation (Figure 5B). This degree of reduction differed moderately, but seemingly reproducibly, from the diminishment by about 40–50% that one could determine for TPR's NE-associated amounts in the ZC3HC1 KO cells of different cell lines, including HCT116, or after having achieved ZC3HC1 deficiency by RNAi (Gunkel *et al.*, 2021; our unpublished data). However, we did not regard these differences as inconsistent with each other, as will be discussed further below.

In its overall microscopic appearance, the redistribution of notable amounts of TPR from the NE into the nucleoplasm upon induced ZC3HC1 degradation appeared to be essentially indistinguishable from what we had already seen in WT cells after several days of ZC3HC1 RNAi and in ZC3HC1 KO cells. However, in at least one aspect, the current result differed from the two latter cases in which most soluble TPR likely had never been NB associated. In the ZC3HC1 RNAi and ZC3HC1 KO cells, such soluble TPR could readily be extracted by standard cell fractionation protocols using detergent-containing NB-s buffers (our unpublished data but see Figure 1D and Supplemental Figure S1F). By contrast, when applying the same fractionation conditions after degron-mediated ZC3HC1 elimination, the initially NB-associated and then detached TPR pool 2 was hardly extractable as soluble polypeptides (Figure 5C). While one can contemplate why this might be (Supplemental Information 8), it still needs to be experimentally determined what causes the detached TPR polypeptides' poor extractability.

The main finding of these degron experiments, though, namely the essentially instantaneous detachment of large TPR amounts from the NE concomitant to the loss of ZC3HC1, could now no longer be explained by other imaginable scenarios that RNAi and gene disruption experiments had not been able to exclude (e.g., Gunkel *et al.*, 2021, and as discussed further below). Instead, the current finding firmly argued for some direct role of ZC3HC1 in keeping subpopulations of TPR appended to the NB also in vivo, with ZC3HC1 acting thereby as a structural element that stabilizes direct interactions between the TPR polypeptides or functions as a linker between them.

Such ZC3HC1-dependent interconnecting of TPR polypeptides would not even need to occur at the NB proper, as revealed by an experiment combining NUP153 RNAi and degron-mediated ZC3HC1 degradation (Figure 6). KD of NUP153 was already known to cause local subcellular accumulations of TPR in either cytoplasmic or nuclear foci, which formerly had been referred to as aggregates (Hase and Cordes, 2003). With such foci now also found positive for ZC3HC1 (Figure 6 and our unpublished data), and with such TPR-containing foci never seen upon KD or KO of ZC3HC1 (e.g., Gunkel *et al.*, 2021; our unpublished data), we wondered whether ZC3HC1 might even play a direct role in keeping TPR agglomerated in such foci.

To address this question, we performed NUP153 RNAi in the ZC3HC1-sfGFP^{L9mIAA7} cell line. In the resulting NUP153-deficient cells, and in the absence of auxin, this again came along with TPR and ZC3HC1 mostly no longer NPC appended but colocalizing in multiple foci instead, with most here located in the cytoplasmic compartment (Figure 6). Strikingly then, upon treatment with auxin, apparently resulting in the degradation of most of the initially foci-positioned ZC3HC1, the foci too were essentially no longer visible. Their disappearance, in turn, was accompanied by the apparent release of the initially there-located TPR into solution, the nuclear import of the then-soluble TPR polypeptides, and their distribution throughout the nucleoplasm in such an absence of NUP153 and ZC3HC1 (Figure 6).

Altogether, these experiments have proven that ZC3HC1 is a structural element that allows for the interconnection of large amounts of TPR and is essential for keeping such TPR ensembles place bound, irrespective of whether they occur at their natural sites at the NB or even at artificial ones elsewhere within the cell.

DISCUSSION

ZC3HC1 is a novel, second structural element of the NB

In the current study, we have demonstrated that protein ZC3HC1 is a bona fide structural element of the NB by dissecting the process leading to the NB residency of the ZC3HC1-dependent TPR polypeptides. Specifically, we have systematically scrutinized whether ZC3HC1 is involved 1) in recruiting such TPR amounts to the NB, 2) in appending them to TPR polypeptides already present at the NPC, and 3) in then keeping the additional ones stably NB associated.

The combination of different experimental approaches allowed for addressing the temporal order of the interactions underlying the reciprocal dependence of ZC3HC1 with TPR. These included assembly experiments, both in vivo and in vitro, which allowed for studying these interactions in a stepwise manner. Furthermore, the inducible, rapid, and complete degron-mediated degradation of ZC3HC1 made it possible to assess this protein's contribution to maintaining the TPR subpopulations' residency at the NB. All these approaches had in common that they allowed for a close spatiotemporal correlation between the addition or removal of ZC3HC1 and the resultant impact on the ZC3HC1-dependent pool of TPR and its NB association.

While former findings based on RNAi-mediated ZC3HC1 KD and *ZC3HC1* gene disruption had already revealed that the presence of ZC3HC1 in cultured cells is required for subpopulations of TPR to occur appended at the NB (Gunkel *et al.*, 2021), it had remained elusive how ZC3HC1 would contribute to such a positioning of TPR pool 2 polypeptides. The formerly observed ZC3HC1 deficiency phenotypes had manifested themselves only time delayed, with the cells first having run through mitosis and thus through NB disassembly and reassembly. Therefore, it had not been possible to unequivocally attribute to ZC3HC1 a role in either the recruitment and appendage or the stable positioning of such additional TPR amounts at the NB.

Such uncertainty and caution in data interpretation were not unfounded because we had also noted that other proteins appeared only transiently involved in some stages of the NB assembly process (our unpublished data). While some of these interactions might be required for adopting specific TPR conformations and NB arrangements as a prerequisite for further assembly steps, none of these other proteins could so far be classified as structural components of the NB, unlike ZC3HC1.

Another reason for caution was the example of the multifaceted relationship between TPR and the NPC protein NUP153. This nucleoporin was, until then, the only other of TPR's published direct binding partners that had been shown to play a role in the NB assembly process. NUP153 is thereby either directly or indirectly involved in recruiting TPR pool 1 polypeptides and in attaching them to those NPCs that are assembled either after mitosis or in interphase (Walther *et al.*, 2001; Hase and Cordes, 2003; Mendjan *et al.*, 2006; Sabri *et al.*, 2007; Mackay *et al.*, 2010; Umlauf *et al.*, 2013; Vollmer *et al.*, 2015; Larrieu *et al.*, 2018; Supplemental Information 6). On the other hand, though, NUP153 was seemingly no longer required by TPR once the latter had been anchored to the NPC's NR (Lussi *et al.*, 2010; Duheron *et al.*, 2014; our unpublished data), which appeared to be in line with NUP153 and TPR having different

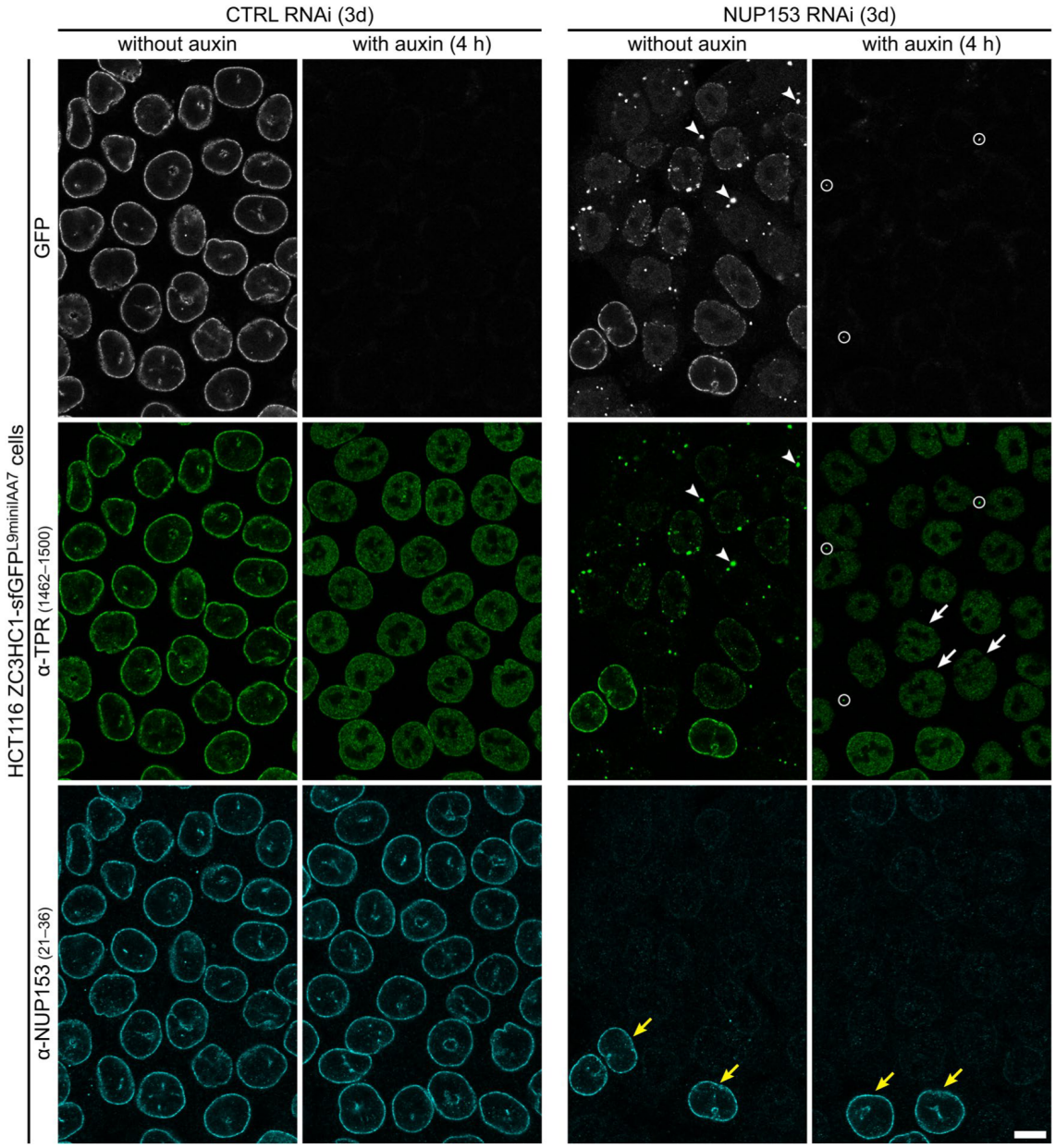

FIGURE 6: Ensembles of degron-tagged ZC3HC1 and TPR, remote from the NB due to NUP153 deficiency, are rapidly disassembled upon auxin-induced ZC3HC1 degradation, which results in TPR polypeptides being unleashed again. IFM of ZC3HC1-sfGFP^{L9mIAA7} HCT116 cells treated with nontarget control (CTRL) or NUP153 siRNAs and, at day 3 posttransfection, with DMSO or with auxin for 4 h, with specimens then analyzed in parallel, using identical microscope settings. Upon NUP153 RNAi, only traces of NUP153 immunolabeling were present at most of the cells' NEs; the usually bright NE staining for NUP153 was visible only in cells that had remained nontransfected (some marked by yellow arrows), here shown as a reference. In the NUP153-deficient cells, NE staining for TPR and ZC3HC1 was conspicuously reduced, with the latter two proteins then colocalizing, in the absence of auxin, in numerous, here primarily cytoplasmic foci (some marked by arrowheads). Note that ZC3HC1 and such foci were hardly detectable anymore (some small remnants encircled) after auxin treatment, with TPR then appearing distributed throughout the NUP153- and ZC3HC1-deficient cells' nucleoplasm (some marked by white arrows). Bar, 10 μm.

anchor points at the NR (Supplemental Information 6). However, because NUP153 RNAi phenotypes relating to TPR:NUP153 interactions at different points of the cell cycle had also varied depending on cell type, duration of the RNAi experiment, and time point of inspection, the various cause-effect relationships observed upon such NUP153 RNAi also had to be interpreted with caution, until recently. Eventually, clarification was provided by a groundbreaking study (Aksenova *et al.*, 2019, 2020) in which a degron-tagged version of Nup153 had been rapidly eliminated by induced degradation, thus causing an immediate phenotype. These experiments proved that NUP153, while required for NB formation and processes leading to NPC appendage of TPR, was indeed not essential for maintaining the TPR polypeptides' anchoring to the NPC.

Hence, such dispensability of NUP153 for keeping bound TPR polypeptides in place, in addition to it not being an NB protein itself and not depending on TPR for its own binding to the NPC, clearly

distinguishes NUP153 from ZC3HC1. In fact, the detachment of essentially all T2 polypeptides from the NE upon the degron-mediated rapid elimination of ZC3HC1 manifested the latter, unlike NUP153, as a structural NB component.

We regard the latter conclusion as not in conflict with the current study's finding that the degron-mediated ZC3HC1 degradation led to somewhat more TPR detached from the NE than upon ZC3HC1 RNAi or in ZC3HC1 KO cells (Gunkel *et al.*, 2021; our unpublished data). Instead, we consider it conceivable that the rapid elimination of ZC3HC1 could have even affected the NPC association of some of the T1 polypeptides that are usually appended to the NPC independently of ZC3HC1. Even without an experimental data-based explanation currently available for these moderate differences, we can imagine, for example, that a proteasome degrading an AID-tagged ZC3HC1 might also consume the one or other T1 polypeptide if some of the degron-tagged ZC3HC1 polypeptides might be very tightly bound to them. We regard such a scenario as not entirely unreasonable, given former findings that a degron-tagged sdAb can confer degradation of its nontagged binding partner if tightly bound to it (e.g., Daniel *et al.*, 2018). On the other hand, however, one should also keep in mind that such codegradation of nontagged binding partners does not appear to happen for other pairs of nontagged and degron-tagged interaction partners (e.g., Beer *et al.*, 2019). We can thus alternatively also imagine that the T1 polypeptides and the residual NB scaffold, once rapidly stripped of all ZC3HC1 and T2 polypeptides, might be generally less durable and more prone to disintegration than NBs built from the ground up in the absence of ZC3HC1.

The results of the current study's assembly experiments further indicated that ZC3HC1 is not merely a structural element required for keeping T2 polypeptides positioned at the NBs in proliferating cells but also needed for the actual recruitment and appendage of such TPR polypeptides. This might appear unavoidable for a structural protein required for maintaining the integrity of higher-order protein ensembles because one could imagine that its presence is also a prerequisite for successful recruitment and appendage of the other proteins. However, we regard it as appropriate to distinguish carefully between recruitment, appendage, and maintenance in the context of the NB's assembly and the maintenance of its higher-order arrangements. Such assemblies of TPR polypeptides appear more complex and dynamically variable than one might have formerly anticipated.

In fact, we can easily imagine that additional proteins exist that are not essential for the NB assembly process and the initial appendage of additional TPR amounts to the NB, but that also play, in addition to ZC3HC1, a role in maintaining the TPR polypeptides' relative positions, once they occur appended to the NBs. Among the candidates conceivable are various nucleic acid–binding proteins, including DNA-binding proteins that detach from nuclease-treated NEs together with TPR, ZC3HC1, and other known NB proteins, upon the disintegration of NBs in different cell types (our unpublished data). We can now conceive a scenario in which the one or other protein capable of interacting with both TPR and nucleic acids might additionally stabilize the NB via lateral interactions with neighboring chromatin, possibly even in a manner varying between different cell types. Again, however, we currently do not regard such other proteins as additional structural elements of the NB, unlike ZC3HC1.

A methodological toolbox for NB research

The type of in vivo and in vitro assembly experiments presented in the current study might also help answer some of the still open questions regarding the contributions of several different proteins, including NB components and other proteins like NUP153, to specific steps in the NB assembly process. We regard these approaches, in which NE scaffolds are used as assembly platforms for ectopically expressed WT proteins and their mutant versions, as suitable for providing insight into how the stepwise interactions between the NPC and NB components and the other NB-interacting proteins take place. While it will not be possible to generate CRISPR/Cas9-edited KO cell lines for every NPC, NB, and NB-associated protein of interest, because some of them are essential, NEs can also be cleared of a target protein by the protein's RNAi-mediated KD or its degron-mediated degradation, once a corresponding CRISPR/Cas9-edited cell line is available. For example, in the case of NUP153, one could create NEs free of NUP153 and NBs via degron-mediated coelimination of NUP153 and TPR, which could then be used for the stepwise readdition of recombinant versions of NUP153 and NB components.

We can also imagine using the NE scaffolds, then with complete NBs, as platforms suited for screening and identifying proteins that interact with the NB only as a structural entity. Circumstantial evidence (our unpublished data) suggests that some transiently NB-interacting proteins can interact with some of the NB's components only when these are part of the NB's higher-order structural arrangements. Such interactions would thus not be readily identifiable by conventional affinity chromatographic approaches or by other means merely based on pairwise interactions, for example, as with yeast two-hybrid methodology.

Furthermore, concerning the NB research–related genes of interest and their tagging with the sfGFP^{L9mIAA7} cassette, one can imagine how the resulting cell lines can be used versatilely. Apart from the induced rapid degradation of the tagged proteins, to study resulting phenotypes, such lines will also allow for the standardized use of GFP-specific sdAbs, not only for the immunoprecipitation of the tagged proteins but also for their visualization at higher resolution by superresolution microscopy.

Beyond that, we propose using such sfGFP^{L9mIAA7}-expressing cell lines, especially when corresponding cell lines of different germ layers and tissue origins are available to be used in parallel, to gain further insight into the standard and the cell-type–specific repertoire of proteins that interact with the NB and its appended structures. Such distinction will be achievable, for example, by mass spectrometry, when inspecting the protein composition of the lamina-NPC-NB (LNN)–enriched materials isolated from such cells before and after induced degradation of different NPC and NB proteins. This has been exemplified in the current study by the degron-mediated degradation of TPR and resulting loss of NB proteins like ZC3HC1 from such LNN materials.

Systematically investigating this in not only one but several cell lines, including correspondingly CRISPR/Cas9-edited stem cells, should contribute to further distinguishing between those proteins that one would rate as universal NB-resident components and those that reside at the NBs of only specific cell types. Furthermore, applying several different LNN isolation procedures in parallel might also provide the inventory of those proteins that only transiently interact with the NB yet exhibit some enrichment at this site. Moreover, systematically comparing populations of quiescent and cell-cycle–synchronized cells should provide insight into possibly cell-cycle-phase–specific interactions between the NB components and other proteins. Finally, such sfGFP^{L9mIAA7}-expressing cell lines might enable studies of potential changes in the NB's interactome under different cellular stress conditions.

Altogether, such subtractive proteomics and interactomics based on degron-mediated target protein elimination would complement and exceed a related approach of comparing NEs with and without NBs in which the latter had been detached by physicochemical means from the NEs of *Xenopus* oocytes, resulting in the initial identification of ZC3HC1 as an NB-resident protein (Gunkel *et al.*, 2021).

The open questions of how and how many of the nonessential ZC3HC1 polypeptides keep which numbers of TPR polypeptides bound where at the NB in what type of arrangements, and why

The current study does not yet permit unambiguously telling how ZC3HC1 exerts its function as a structural element required for keeping the T2 polypeptides bound at the NB, as the data do not yet allow for unambiguously distinguishing between different scenarios. On the one hand, ZC3HC1 could be a protein whose interaction with T1 polypeptides would force the latter into a specific conformation, only thereby forming a platform that would allow for direct interactions between T1 and T2 polypeptides. Alternatively, ZC3HC1 may form, for example, a flange or socket that would allow for some direct interaction between the T1 and T2 polypeptides, with possibly the latter mounted on the former. On the other hand, though, it is also tempting to imagine ZC3HC1 as an interconnector positioned between the different populations of TPR polypeptides, with such a setup then not necessarily requiring any direct contact between TPR pools 1 and 2. However, which of these scenarios, not all of which would be mutually exclusive, will eventually hold will have to be the topic of studies still to come.

Such studies will also need to delineate those parts of ZC3HC1 and TPR that enable them to engage in such a relationship. In addition, they will have to provide the total copy numbers for those ZC3HC1 and TPR polypeptides that engage in such interactions at the NB, as only such numbers will eventually allow sketching which type of arrangements and constellations among these proteins at the NB will be numerically possible.

Furthermore, because the current evidence already hints at different subpopulations of TPR that occur NB associated, their copy numbers, too, need to be known. While the current study refers to at least two major TPR subpopulations, which we called T1 and T2 for simplification, data from further experiments, in which we have systematically disassembled the NB stepwise in more detail, have hinted at even further subpopulations within those of T1 and T2. For example, in the case of the T1 pool, this could mean that it might actually be composed of two equally large subpopulations, T1a and T1b (Gunkel *et al.*, 2021; our unpublished data). Similarly, circumstantial evidence, in both the recent study (Gunkel *et al.*, 2021) and the current one (Supplemental Figure S6), points to also the existence of ZC3HC1 subpopulations. These appear to engage in different interactions with TPR and the NB, with each ZC3HC1 subpopulation perhaps having a distinct task while acting cooperatively, or instead sequentially, in the TPR assembly processes. The data of systematic cell fractionation and NB disassembly experiments (Gunkel *et al.*, 2021; our unpublished data) also hint at NB-associated ZC3HC1 subpopulations with different dissociation characteristics, and at some point, the copy numbers for each of these different subpopulations will also need to be determined.

Another question among the central ones regarding the NB's architecture in the proliferating human cell is how the ZC3HC1-recruited TPR populations are arranged and positioned relative to those TPR polypeptides that are anchored to the NPC independently of ZC3HC1. In the one scenario, one can imagine both pools representing components of the same structure commonly regarded as the prototypic NB, with both the T1 and T2 polypeptides perhaps even longitudinally aligned. On the other hand, it is tempting to envision the T2 polypeptides as attached to the NB in such a manner that would allow them to project away from the NB and reach out further into the nuclear interior, similar to arrangements described for NBs in *Xenopus* oocytes (e.g., Gunkel *et al.*, 2021). However, to address this and further questions regarding the NB's assembly blueprint and final architecture, one will need to dissect the NB assembly process in further molecular detail and study further mutant versions of ZC3HC1 and those of TPR. Moreover, one will also need to microscopically visualize the arrangement of the different TPR subpopulations relative to each other and ZC3HC1. The emerging novel methodologies in superresolution microscopy might now allow for resolving these proteins' positions relative to the NPCs in different human cell lines.

Perhaps the most pressing question is why evolution has decided to stick with ZC3HC1 in a wide range of species, even though the protein appears to be dispensable for all those species in which the corresponding homologue hitherto has been eliminated experimentally (Gunkel *et al.*, 2021, and references therein). For example, such dispensability also holds for *Saccharomyces cerevisiae* Pml39p, a protein that binds to the yeast's TPR homologues Mlp1p and Mlp2p (Palancade *et al.*, 2005) and that we found to be the budding yeast's sole homologue of ZC3HC1 (Gunkel *et al.*, 2021; our unpublished data). Moreover, even evolution itself has sometimes allowed for again discarding an initially present ZC3HC1 homologue, with this having happened and seemingly still happening within some subphyla, orders, or even families of organisms. Such an evolutionary fate of ZC3HC1 can be reconstructed, for example, in insects. Here, almost all orders, including Diptera and thus also *Drosophila*, lack an apparent ZC3HC1 homologue, while it is unambiguously still present in some species of other insect orders and while likely functionally intact ZC3HC1 homologues are omnipresent in all other subphyla of the Arthropoda (Gunkel *et al.*, 2021; our unpublished data).

Such findings raise the question of what the additional amounts of TPR are good for in those organisms in which ZC3HC1 acts as a structural element appending them to the NB; and conversely, why ZC3HC1-deficient organisms have adapted to getting along without such additional amounts of TPR, provided that such species have not come up with some protein functionally analogous to ZC3HC1 or some other mechanism of appending more TPR to their NBs.

Recently, several tasks have been outlined that one could imagine for the ZC3HC1-dependent populations of TPR polypeptides (Gunkel *et al.*, 2021). For example, apart from potential contributions to the NB's overall structural stability, one scenario suggested that ZC3HC1 allowed for increasing the number of TPR polypeptides for the sake of these acting as either transient or more lasting binding sites at the NB for yet other molecules, with the copy numbers of such additional TPR polypeptides perhaps even modifiable upon demand. Among the TPR-interacting candidate molecules in such a scenario, one could imagine proteins involved in transcription regulation, replication, and perinuclear chromatin organization. Such interactions would be in keeping with numerous studies in which the NB and TPR homologues have been found engaging in different types of interactions with NB-neighboring chromatin and a subset of genes. For example, such findings hold for metazoans and *Arabidopsis* (e.g., Mendjan *et al.*, 2006; Skaggs *et al.*, 2007; Krull *et al.*, 2010; Vaquerizas *et al.*, 2010; Myers *et al.*, 2016; Zhang *et al.*, 2016; Pérez-Garrastachu *et al.*, 2017; Yang *et al.*, 2017; Raich *et al.*, 2018; Su *et al.*, 2018; Boumendil *et al.*, 2019; Cohn *et al.*, 2020;

Aleman *et al.*, 2021; Kosar *et al.*, 2021; Uhlířová *et al.*, 2021; Wu *et al.*, 2021; our unpublished data). Similarly, they also hold for *S. cerevisiae*, with its TPR homologues Mlp1p/Mlp2p and proteins associated with them (Casolari *et al.*, 2004; Cabal *et al.*, 2006; Dieppois *et al.*, 2006; Schmid *et al.*, 2006; Brickner *et al.*, 2007; Luthra *et al.*, 2007; Tan-Wong *et al.*, 2009; Bermejo *et al.*, 2011; Texari *et al.*, 2013; García-Benítez *et al.*, 2017).

This scenario, though, leads us back to the question of why ZC3HC1-deficient organisms like *Drosophila*, in which interactions between *Drosophila*'s TPR homologue Mtor and the autosomes and male X-chromosome occur nonetheless (e.g., Mendjan *et al.*, 2006; Vaquerizas *et al.*, 2010; Raich *et al.*, 2018; Aleman *et al.*, 2021), would not require more TPR appended to their NBs, and why such organisms do well or perhaps even better without them. The answers to such fundamental questions might eventually explain why evolution has decided that we and other species, by contrast, should rather hang on to ZC3HC1 as a second structural element of the NB.

MATERIALS AND METHODS

Antibodies

All specifications regarding antibodies used in this study are provided in Supplemental Table S1. Among these are novel *Hs*TPR antibodies, all raised in rabbits, that were used for immunoaffinity depletion of TPR from human cell extracts (see below). One of these TPR antibodies was obtained after immunization with a chemically synthesized peptide, corresponding to *Hs*TPR aa 2147–2163 and phosphorylated at S2155. The others were obtained after immunization with recombinant fragments of *Hs*TPR, followed by isolating subpopulations of peptide-specific antibodies from the resulting sera, using sets of overlapping peptides for affinity chromatography, as recently described for collections of *Xl*TPR peptide antibodies (Gunkel *et al.*, 2021).

Cell culture, auxin treatment, RNAi, synchronization, and transfections

All cell lines used in this study, including those generated by CRISPR/Cas9 editing, and their growth conditions, including types of media used, are listed in Supplemental Table S2. Cell cycle synchronization was performed as described (Gunkel *et al.*, 2021). To initiate auxin-induced degradation, we first added the auxin indole-3-acetic acid (I5148; Sigma-Aldrich) from a 500 mM stock solution in dimethyl sulfoxide (DMSO) to the cell-free cell culture medium at a concentration of 0.5 mM, followed by incubation at 37°C and 5% CO_2 for 30–60 min. The stock solution had been freshly prepared or frozen for no longer than 1 week and then thawed. Next, the prewarmed, auxin-supplemented medium was used to replace the medium of the cells. A prewarmed medium supplemented with auxin-free DMSO was applied concomitantly to the control population cells. Transfections of HCT116 cells with small interfering RNAs (siRNAs; Silencer Select negative controls #1 and 2 [#4390843 and #4390846] and Silencer Select siRNAs targeting *Hs*NUP153 [s19374 [CGAAAAUCUCUCUACCGAU] and s19376 [CAGUCUAAACUACGAAAUA]]; Ambion, Austin, TX) were performed as described (Gunkel *et al.*, 2021). For the transfections of HeLa with mammalian expression vectors presented in Figure 1, we used PolyJet (SignaGen Laboratories, Frederick, MD) as the transfection reagent, following the manufacturer's instructions. For transfections of HeLa and HCT116 cells in the course of the gene-editing procedures, see further below. For large-scale transfections of the adherent HEK293T cells for the ectopic expression of proteins for the in vitro assembly experiments, we followed a transfection protocol (Reed *et al.*, 2006) using linear 25 kDa polyethylenimine (PEI; Polysciences Europe GmbH, Hirschberg, Germany). We adjusted this protocol for 10 cm culture dishes with about 50–70% cell density, with these and further modifications already described (Gunkel *et al.*, 2021), yet harvesting cells in the current study 16–21 h after the initial transfection.

IFM and live-cell imaging of cultured cells

For standard IFM, cells were fixed for 30 min with 2.4% of freshly prepared and methanol-free formaldehyde (FA) in phosphate-buffered saline (PBS), followed by quenching with 50 mM NH_4Cl in PBS and permeabilization with 0.25% Triton X-100 (TX-100) in PBS for 5 min. In cases in which detergent-permeabilization was carried out before FA fixation (Figure 1D), cells were treated with 0.25% TX-100 in a temporarily tNB-s buffer for 3 min, the latter here composed of PBS to which $MgCl_2$ was freshly added to a final concentration of 10 mM. This step was followed by fixation in tNB-s buffer and then by quenching with NH_4Cl in PBS, yet omitting subsequent treatments with detergents. Blocking and antibody incubations were performed with 1% bovine serum albumin (BSA) in PBS, with Hoechst 33342 (1 µg/ml) for DNA staining added during the incubation with fluorophore-coupled secondary antibodies. The immunolabeled specimens were mounted in SlowFade Gold or Diamond Antifade Mountant (Invitrogen, Carlsbad, CA), the latter used for FA-fixed GFP-tagged specimens and the subsequent inspection of their GFP signals too. For live-cell imaging, cells were grown on four- or eight-well ibidi glass-bottom (#1.5H) µ-slides (ibidi, Martinsried, Germany), using either Leibovitz's L-15 medium (Sigma-Aldrich) or the live-cell imaging medium FluoroBrite DMEM (Gibco). An improved version of SiR-Hoechst (Bucevičius *et al.*, 2019), kindly provided by Gražvydas Lukinavičius (Max Planck Institute for Multidisciplinary Sciences, Göttingen, Germany), was used for DNA staining of living cells. All cells, that is, the immunolabeled and the intact live cells, were inspected with a Leica TCS SP5 or SP8 confocal laser-scanning microscope (Leica Microsystems, Wetzlar, Germany) equipped with a 20× and a 63× oil immersion objective (Leica Microsystems). The color lookup table (LUT), named C3_linear-protanopic-deuteranopic, was obtained from the NeuroCyto Lab (University of Marseille, France; https://sites.imagej.net/NeuroCyto-LUTs).

Cell fractionation and immunoblotting

Fractionation of confluent, not synchronized populations of HCT116 cells to obtain, for immunoblotting (IB), a fraction of soluble proteins released upon extraction with TX-100 and a nonsoluble LNN-enriched fraction, was in principle as described (Gunkel *et al.*, 2021), with only minor modifications. We thereby applied conditions that allow for maintaining the interactions of TPR and ZC3HC1 with the NBs and the LNN-enriched material. In brief, washed cells of lines HCT116 MCL and sfGFP^{L9mIAA7}-TPR, which had been treated with auxin or not, were sedimented by 800 × *g* centrifugation for 3 min. Next, the cells were resuspended in 20–22°C-warm NB-s solution containing 41.5 mM KCl, 8.5 mM NaCl, 5 mM $MgCl_2$, 2.5 mM ethylene glycol bis(2-aminoethyl)-tetraacetic acid (EGTA), 2 mM dithiothreitol (DTT), 10% sucrose, 20 mM HEPES, pH 7.5, 0.25% TX-100, and cOmplete EDTA-free protease inhibitor cocktail (Roche, Basel, Switzerland), followed by incubation for 4 min. The cell suspensions were then centrifuged at 20,000 × *g* and RT for 3 min. Cells of line HCT116 ZC3HC1-sfGFP^{L9mIAA7} were handled similarly, except for incubating them, after having treated them in parallel with and without auxin, in the NB-s buffer containing TX-100 for 15 min. The fractionations of HeLa and HEK293T cells for the assembly assays presented in Figures 2 and 3 were performed as explained further below, and SDS–PAGE and IB were as described recently (Gunkel *et al.*, 2021).

In vitro assembly experiments with ZC3HC1-deficient NEs and fluorescent protein-tagged ZC3HC1 and TPR polypeptides

For preparing TPR-free cell extracts with either the mCherry-tagged WT or C429S mutant version of ZC3HC1, up to about 1.4×10^8 adherent HEK293T cells were transiently transfected with corresponding expression vectors (see Supplemental Table S3) and harvested 16–21 h later. Cells were sedimented by a 3 min centrifugation at 1000 × *g* and resuspended in an NB-s buffer, here called assembly buffer, composed of 88 mM KCl, 22 mM NaCl, 10 mM $MgCl_2$, 10 mM potassium sodium phosphate (4:1 molar ratio of K_2HPO_4/KH_2PO_4:Na_2HPO_4/NaH_2PO_4), pH 6.8. The cells were then recentrifuged at 1500 × *g* and RT for 2 min, resuspended at a volume ratio of about 1:4 between pellet volume and solution, in assembly buffer supplemented with cOmplete Mini EDTA-free protease inhibitor cocktail (Roche) and 0.05% digitonin, for permeabilization at RT for 3 min. They were subsequently centrifuged at 20,000 × *g* and RT for 2 min, followed by recentrifuging the resulting supernatants at 200,000 × *g* and at 4°C for 10 min. The then obtained solutions were rotated at RT for 20 min together with protein A–coupled magnetic Dynabeads (Invitrogen, Carlsbad, CA) that had been loaded beforehand with a collection of five different rabbit antibodies targeting different parts of *Hs*TPR (see Supplemental Table S1). Such loading was performed in the assembly buffer containing 0.02% Tween-20 at RT for 15 min, followed by several washes in the same buffer. For the immunodepletion of such soluble HEK293T extracts, then generally corresponding to still about $5–9 \times 10^7$ cells, a total of up to about 18–21 µg of anti-TPR immunoglobulin Gs was used, with each of the five different *Hs*TPR antibodies contributing different amounts, ranging between 2.9 and 5.8 µg. The antibodies' corresponding total of copy numbers coupled to the magnetic beads was calculated to exceed the maximally expectable total numbers of soluble TPR dimers within the cell extracts at least 200-fold. Following the magnetic removal of the beads, the solutions were directly used for the interaction experiments; yet later on, they were always controlled by IB to have been devoid of TPR. The ZC3HC1-free cell extracts containing the sfGFP-tagged TPR polypeptides, on the other hand, were obtained from one of the sfGFP-TPR–expressing HeLa ZC3HC1 KO cell lines in which substantial amounts of TPR that usually occur NE associated in WT cells are distributed throughout the nuclear interior in a soluble form instead. To this end, about 1×10^8 cells from subconfluent populations, that is, from such in which cell sizes were still notably larger than in highly confluent populations of HeLa, were first washed in assembly buffer. They were then sedimented by centrifugation at 1000 × *g* for 3 min, resuspended in assembly buffer, and recentrifuged for 2 min at 1000 × *g*. Next, they were resuspended in assembly buffer, supplemented with cOmplete Mini EDTA-free protease inhibitors, at a volume ratio of about 1.25:1 between buffer and pellet volume, the latter though still containing buffer from the preceding washing step so that the actual ratio between buffer and total cell volume came rather close to 1.8:1. All steps were performed at RT. About 5×10^7 cells as 325 µl suspensions in 1.5 ml safe-lock tubes (Eppendorf AG, Hamburg, Germany) were ruptured by brief pulsed sonication at RT using the ultrasonic homogenizer SONOPULS mini20, equipped with an MS 2.0 sonotrode (Bandelin Electronic GmbH, Berlin, Germany). For such sonication, we applied conditions (sonotrode immersion depth of 1 mm, amplitude setting 50%, pulsating mode, a 15-s total length of operation, with pulses of 0.5 s separated by pauses of 1 s), which we had heuristically determined by series of trial-and-error experiments. Such conditions allowed for an adequate, that is, a probably complete rupturing of the suspended HeLa cells' nuclei without causing disruption of the NEs primarily into fragments no longer sedimentable at 20,000 × *g*, while at the same time allowing for minimizing energy input and keeping the mean rise in temperature within the suspension below 2°C. The cell suspensions were then centrifuged at RT and 20,000 × *g* for 2 min, followed by recentrifugation of the resulting supernatant at 4°C and 200,000 × *g* for 10 min. Supernatants obtained in such a way, free of any detectable NE fragments but containing soluble sfGFP-TPR polypeptides, were used for the assembly assays straight away. Note that for time reasons, the preparation of such freshly prepared HEK293T and HeLa cell extracts for their direct use in the assembly experiments required two persons' work efforts in parallel. For preparing the NEs as assembly platforms, HeLa ZC3HC1 KO cells were grown on eight-well ibidi µ-slides with ibiTreat bottom (ibidi) to which HeLa cells, unlike HCT116, tightly adhered during the subsequent treatments. Populations of 50–70% cell density were then permeabilized with detergent just before the addition of the cell extracts. To this end, the cells were incubated for about 2 min to maximally 3 min in the assembly buffer containing 0.25% TX-100 and Hoechst 33342 (1 µg/ml), accompanied by gentle rocking, followed by three washes with detergent-free assembly buffer, with the first wash step for 2 min still containing the DNA dye, then omitted from the next steps. All subsequent incubations with the mCherry-ZC3HC1- and the sfGFP-TPR–containing solutions and all washes, using the detergent-free assembly buffer supplemented with cOmplete Mini EDTA-free protease inhibitors, were performed at RT. After having loaded the nuclei with the recombinant polypeptides, the specimens were inspected with a Leica TCS SP8 confocal laser-scanning microscope (Leica Microsystems, Wetzlar, Germany). All images of mCherry fluorescence, respectively those of sfGFP, were acquired with identical microscope settings and with reduced laser power, as compared with IFM images, to minimize pronounced bleaching in the absence of anti-fade media. The signal brightness of all raw images was then enhanced electronically, which was done in the same manner for each series of corresponding images. To this end, all corresponding color images of either mCherry or sfGFP were first assembled into one image and then converted to the 8-bit grayscale of 0–255. Using the Multiply command in the Math Submenu of the ImageJ/Fiji software (version 2.0.0-rc-64/1.51t; National Institutes of Health, USA), each pixel value of this composite image was then multiplied by the same multiplication factor. This constant multiplication of pixel intensities was the only image processing conducted for the in vitro assembly experiments. With less than 0.05% of each image's pixels finally reaching a value of 255, this procedure allowed the signal intensity relationships between the electronically brightness-enhanced images to remain essentially the same as between the corresponding raw images beyond their background zero values.

Genomic editing in human cell lines

The deletion of ZC3HC1 gene segments in human cell lines, using CRISPR/Cas9 technology and following the Cas9 double-nickase approach with pairs of single guide RNAs (sgRNA; Ran *et al.*, 2013a), was performed as described in detail recently (Gunkel *et al.*, 2021). This approach was also used for tagging the TPR and ZC3HC1 alleles with the ORF for sfGFP or variants thereof. Novel pairs of sgRNAs, with sequences complementary to the genomic regions at which the integration was to occur (for sequences, see Supplemental Table S4; also see Supplemental Figures S1, S2, S8, and S9), were once again designed by using the CRISPR Design tool formerly provided online by the Zhang laboratory (Hsu *et al.*, 2013). The synthesized sgRNAs were then cloned into the bicistronic Cas9n expression vector pSpCas9n(BB)-2A-Puro (PX462) V2.0 (Ran *et al.*, 2013b) kindly provided by Feng Zhang (Broad Institute, Cambridge, MA;

see Supplemental Table S3). Further details were as described (Gunkel *et al.*, 2021), except for using only one pair of sgRNAs and thus two sgRNA/Cas9n vectors in the current study per integration site. Cultured cells were then transfected with the GFP-donor plasmid and the two target site–specific sgRNA/Cas9n vectors, using PolyJet (SignaGen Laboratories) for transfection of HeLa cells and FuGene HD (Promega Cooperation, Madison, WI) for HCT116, according to the manufacturer's instructions. Three to four days after transfection, the sfGFP-expressing cells were enriched by sorting via flow cytometry using a Bio-Rad S3e cell sorter (Bio-Rad Laboratories, Hercules CA). In some cases, this step was repeated with the first enriched population of GFP-positive cells to sort for the brightest ones, often representing those in which the sfGFP ORF had been integrated into all of the target gene's alleles. These enriched populations were then seeded into 10 cm culture dishes at a low cell density to allow for the growth of monoclonal colonies that could be manually picked and transferred into 15-well µ-slides (µ-slide angiogenesis ibiTreat bottom; ibidi) for further growth. The clones were screened by live-cell imaging, assessing subcellular GFP localization and comparing the different clones' NE-associated GFP brightness under identical microscope settings. The brightest NE-positive clones were selected for colony expansion, followed by further analysis by comparative IFM and IB next to the corresponding progenitor cell line. In addition, all monoclonal populations of the CRISPR/Cas9-edited KO and GFP-expressing cell strains were analyzed by genomic PCR and DNA sequencing of subcloned PCR products (for primers, see Supplemental Table S5). For generating the HCT116 MCL with constitutive *At*AFB2 expression, HCT116 WT cells were transfected with the sgRNA/Cas9 vector (kindly provided by Masato Kanemaki, National Institute of Genetics, Mishima, Japan; see Supplemental Table S3) together with the integration vectors for *At*AFB2-Myc and *At*AFB2-Myc-NLS (based on a vector kindly provided by Elina Ikonen, Faculty of Medicine, University of Helsinki, Helsinki, Finland; see Supplemental Table S3) using the FuGene HD transfection reagent (Promega). As the integration site for the *At*AFB2 cassettes, we chose Adeno-Associated Virus Integration Site 1 (AAVS1) safe-harbor locus (Supplemental Figure S7B). Puromycin (5 µg/ml) was added to select for transfected cells that were grown until monoclonal colonies could be manually picked. IFM was then used to screen the expanded clones for the presence and subcellular distribution of the Myc-tagged *At*AFB2. The eventually selected *At*AFB2-expressing HCT116 clone that we found suitable as the MCL (Supplemental Figure S7C) was used for subsequently integrating the sfGFP^{L9mIAA7} cassette into the alleles of any target gene of interest. For details regarding the design of the sfGFP^{L9mIAA7} cassette, see Supplemental Figures S7–S9 and Supplemental Table S3).

ACKNOWLEDGMENTS

We thank Dirk Görlich for generous support. Furthermore, we acknowledge Gražvydas Lukinavičius, Elina Ikonen, Masato Kanemaki, and Feng Zhang for kindly providing research reagents. In addition, we thank Thomas Güttler, Georg Krohne and Helen Pickersgill for their critical reading of the manuscript.

REFERENCES

Aksenova V, Lee HN, Smith A, Chen S, Bhat P, Iben J, Echeverria C, Fontoura B, Arnaoutov A, Dasso M (2019). Distinct basket nucleoporins roles in nuclear pore function and gene expression: Tpr is an integral component of the TREX-2 mRNA export pathway. BioRxiv, https://doi.org./10.1101/685263.

Aksenova V, Smith A, Lee H, Bhat P, Esnault C, Chen S, Iben J, Kaufhold R, Yau KC, Echeverria C, *et al.* (2020). Nucleoporin TPR is an integral component of the TREX-2 mRNA export pathway. Nat Commun 11, 4577.

Aleman JR, Kuhn TM, Pascual-Garcia P, Gospocic J, Lan Y, Bonasio R, Little SC, Capelson M (2021). Correct dosage of X chromosome transcription is controlled by a nuclear pore component. Cell Rep 35, 109236.

Ashkenazy-Titelman A, Shav-Tal Y, Kehlenbach RH (2020). Into the basket and beyond: the journey of mRNA through the nuclear pore complex. Biochem J 477, 23–44.

Bassermann F, von Klitzing C, Illert AL, Münch S, Morris SW, Pagano M, Peschel C, Duyster J, Klitzing C, Illert AL, *et al.* (2007). Multisite phosphorylation of nuclear interaction partner of ALK (NIPA) at G2/M involves cyclin B1/Cdk1. J Biol Chem 282, 15965–15972.

Bassermann F, von Klitzing C, Münch S, Bai R-Y, Kawaguchi H, Morris SW, Peschel C, Duyster J, von Klitzing C, Münch S, *et al.* (2005). NIPA defines an SCF-type mammalian E3 ligase that regulates mitotic entry. Cell 122, 45–57.

Beer KB, Fazeli G, Judasova K, Irmisch L, Causemann J, Mansfeld J, Wehman AM (2019). Degron-tagged reporters probe membrane topology and enable the specific labelling of membrane-wrapped structures. Nat Commun 10, 1–16.

Bensidoun P, Zenklusen D, Oeffinger M (2021). Choosing the right exit: how functional plasticity of the nuclear pore drives selective and efficient mRNA export. Wiley Interdiscip Rev RNA e1660.

Bermejo R, Capra T, Jossen R, Colosio A, Frattini C, Carotenuto W, Cocito A, Doksani Y, Klein H, Gómez-González B, *et al.* (2011). The replication checkpoint protects fork stability by releasing transcribed genes from nuclear pores. Cell 146, 233–246.

Boumendil C, Hari P, Olsen KCF, Acosta JC, Bickmore WA (2019). Nuclear pore density controls heterochromatin reorganization during senescence. Genes Dev 33, 144–149.

Brickner DG, Cajigas I, Fondufe-Mittendorf Y, Ahmed S, Lee PC, Widom J, Brickner JH (2007). H2A.Z-mediated localization of genes at the nuclear periphery confers epigenetic memory of previous transcriptional state. PLoS Biol 5, 704–716.

Bucevičius J, Keller-Findeisen J, Gilat T, Hell SW, Lukinavičius G (2019). Rhodamine-Hoechst positional isomers for highly efficient staining of heterochromatin. Chem Sci 10, 1962–1970.

Cabal GG, Genovesio A, Rodriguez-Navarro S, Zimmer C, Gadal O, Lesne A, Buc H, Feuerbach-Fournier F, Olivo-Marin J-C, Hurt EC, *et al.* (2006). SAGA interacting factors confine sub-diffusion of transcribed genes to the nuclear envelope. Nature 441, 770–773.

Casolari JM, Brown CR, Komili S, West J, Hieronymus H, Silver PA (2004). Genome-wide localization of the nuclear transport machinery couples transcriptional status and nuclear organization. Cell 117, 427–439.

Cohen RN, van der Aa M, Macaraeg N, Lee AP, Szoka FC (2009). Quantification of plasmid DNA copies in the nucleus after lipoplex and polyplex transfection. J Control Release 135, 166–174.

Cohn GM, Liefwalker DF, Langer EM, Sears RC (2020). PIN1 provides dynamic control of MYC in response to extrinsic signals. Front Cell Dev Biol 8, 1–7.

Cordes VC, Reidenbach S, Rackwitz HR, Franke WW (1997). Identification of protein p270/TPR as a constitutive component of the nuclear pore complex-attached intranuclear filaments. J Cell Biol 136, 515–529.

Daniel K, Icha J, Horenburg C, Müller D, Norden C, Mansfeld J (2018). Conditional control of fluorescent protein degradation by an auxin-dependent nanobody. Nat Commun 9, 3297.

Dieppois G, Iglesias N, Stutz F (2006). Cotranscriptional recruitment to the mRNA export receptor Mex67p contributes to nuclear pore anchoring of activated genes. Mol Cell Biol 26, 7858–7870.

Duheron V, Chatel G, Sauder U, Oliveri V, Fahrenkrog B (2014). Structural characterization of altered nucleoporin NUP153 expression in human cells by thin-section electron microscopy. Nucleus 5, 601–612.

Duheron V, Nilles N, Pecenko S, Martinelli V, Fahrenkrog B (2017). Localisation of Nup153 and SENP1 to nuclear pore complexes is required for 53BP1 mediated DNA double-strand break repair. J Cell Sci jcs.198390.

Frosst P, Guan T, Subauste C, Hahn K, Gerace L (2002). TPR is localized within the nuclear basket of the pore complex and has a role in nuclear protein export. J Cell Biol 156, 617–630.

García-Benítez F, Gaillard H, Aguilera A (2017). Physical proximity of chromatin to nuclear pores prevents harmful R loop accumulation contributing to maintain genome stability. Proc Natl Acad Sci USA 114, 10942–10947.

Gengenbacher A, Müller-Rudorf A, Poggio T, Gräßel L, Dumit VI, Kreutmair S, Lippert LJ, Duyster J, Illert AL (2019). Proteomic phosphosite analysis identified crucial NPM-ALK-mediated NIPA serine and threonine residues. Int J Mol Sci 20, 4060.

Glover DJ, Leyton DL, Moseley GW, Jans DA (2010). The efficiency of nuclear plasmid DNA delivery is a critical determinant of transgene expression at the single cell level. J Gene Med 12, 77–85.

Gossen M, Bujard H (1992). Tight control of gene expression in mammalian cells by tetracycline-responsive promoters. Proc Natl Acad Sci USA 89, 5547–5551.
Gossen M, Freundlieb S, Bender G, Müller G, Hillen W, Bujard H (1995). Transcriptional activation by tetracyclines in mammalian cells. Science 268, 1766–1769.
Gunkel P, Iino H, Krull S, Cordes VC (2021). ZC3HC1 is a novel inherent component of the nuclear basket, resident in a state of reciprocal dependence with TPR. Cells 10, 1937.
Hase ME, Cordes VC (2003). Direct interaction with NUP153 mediates binding of TPR to the periphery of the nuclear pore complex. Mol Biol Cell 14, 1923–1940.
Hase ME, Kuznetsov NV, Cordes VC (2001). Amino acid substitutions of coiled-coil protein TPR abrogate anchorage to the nuclear pore complex but not parallel, in-register homodimerization. Mol Biol Cell 12, 2433–2452.
Heinz N, Schambach A, Galla M, Maetzig T, Baum C, Loew R, Schiedlmeier B (2011). Retroviral and transposon-based tet-regulated all-in-one vectors with reduced background expression and improved dynamic range. Hum Gene Ther 22, 166–176.
Hsu PD, Scott DA, Weinstein JA, Ran FA, Konermann S, Agarwala V, Li Y, Fine EJ, Wu X, Shalem O, *et al.* (2013). DNA targeting specificity of RNA-guided Cas9 nucleases. Nat Biotechnol 31, 827–832.
Illert AL, Kawaguchi H, Antinozzi C, Bassermann F, Quintanilla-Martinez L, Klitzing C, Hiwatari M, Peschel C, de Rooij DG, Morris SW, *et al.* (2012). Targeted inactivation of nuclear interaction partner of ALK disrupts meiotic prophase. Development 139, 2523–2534.
Khmelinskii A, Keller PJ, Bartosik A, Meurer M, Barry JD, Mardin BR, Kaufmann A, Trautmann S, Wachsmuth M, Pereira G, *et al.* (2012). Tandem fluorescent protein timers for in vivo analysis of protein dynamics. Nat Biotechnol 30, 708–714.
Kosar M, Giannattasio M, Piccini D, Maya-Mendoza A, García-Benítez F, Bartkova J, Barroso SI, Gaillard H, Martini E, Restuccia U, *et al.* (2021). The human nucleoporin Tpr protects cells from RNA-mediated replication stress. Nat Commun 12, 3937.
Krull S, Dörries J, Boysen B, Reidenbach S, Magnius L, Norder H, Thyberg J, Cordes VC (2010). Protein TPR is required for establishing nuclear pore-associated zones of heterochromatin exclusion. EMBO J 29, 1659–1673.
Krull S, Thyberg J, Björkroth B, Rackwitz H-R, Cordes VC (2004). Nucleoporins as components of the nuclear pore complex core structure and TPR as the architectural element of the nuclear basket. Mol Biol Cell 15, 4261–4277.
Larrieu D, Viré E, Robson S, Breusegem SY, Kouzarides T, Jackson SP (2018). Inhibition of the acetyltransferase NAT10 normalizes progeric and aging cells by rebalancing the Transportin-1 nuclear import pathway. Sci Signal 11, eaar5401.
Lee SH, Sterling H, Burlingame A, McCormick F (2008). TPR directly binds to MAD1 and MAD2 and is important for the MAD1-MAD2-mediated mitotic spindle checkpoint. Genes Dev 22, 2926–2931.
Li S, Prasanna X, Salo VT, Vattulainen I, Ikonen E (2019). An efficient auxin-inducible degron system with low basal degradation in human cells. Nat Methods 16, 866–869.
Lussi YC, Shumaker DK, Shimi T, Fahrenkrog B (2010). The nucleoporin NUP153 affects spindle checkpoint activity due to an association with MAD1. Nucleus 1, 71–84.
Luthra R, Kerr SC, Harreman MT, Apponi LH, Fasken MB, Ramineni S, Chaurasia S, Valentini SR, Corbett AH (2007). Actively transcribed GAL genes can be physically linked to the nuclear pore by the SAGA chromatin modifying complex. J Biol Chem 282, 3042–3049.
Mackay DR, Makise M, Ullman KS (2010). Defects in nuclear pore assembly lead to activation of an Aurora B-mediated abscission checkpoint. J Cell Biol 191, 923–931.
Mendjan S, Taipale M, Kind J, Holz H, Gebhardt P, Schelder M, Vermeulen M, Buscaino A, Duncan K, Mueller J, *et al.* (2006). Nuclear pore components are involved in the transcriptional regulation of dosage compensation in Drosophila. Mol Cell 21, 811–823.
Merzlyak EM, Goedhart J, Shcherbo D, Bulina ME, Shcheglov AS, Fradkov AF, Gaintzeva A, Lukyanov KA, Lukyanov S, Gadella TWJ, *et al.* (2007). Bright monomeric red fluorescent protein with an extended fluorescence lifetime. Nat Methods 4, 555–557.
Mitchell PJ, Cooper CS (1992). The human tpr gene encodes a protein of 2094 amino acids that has extensive coiled-coil regions and an acidic C-terminal domain. Oncogene 7, 2329–2333.
Myers KN, Barone G, Ganesh A, Staples CJ, Howard AE, Beveridge RD, Maslen S, Skehel JM, Collis SJ (2016). The bornavirus-derived human protein EBLN1 promotes efficient cell cycle transit, microtubule organisation and genome stability. Sci Rep 6, 1–12.
Natsume T, Kiyomitsu T, Saga Y, Kanemaki MT (2016). Rapid protein depletion in human cells by auxin-inducible degron tagging with short homology donors. Cell Rep 15, 210–218.
Niepel M, Molloy KR, Williams R, Farr JC, Meinema AC, Vecchietti N, Cristea IM, Chait BT, Rout MP, Strambio-De-Castillia C (2013). The nuclear basket proteins Mlp1p and Mlp2p are part of a dynamic interactome including Esc1p and the proteasome. Mol Biol Cell 24, 3920–3938.
Niswender KD, Blackman SM, Rohde L, Magnuson MA, Piston DW (1995). Quantitative imaging of green fluorescent protein in cultured cells: comparison of microscopic techniques, use in fusion proteins and detection limits. J Microsc 180, 109–116.
Ouyang T, Bai R-Y, Bassermann F, von Klitzing C, Klumpen S, Miething C, Morris SW, Peschel C, Duyster J, von Klitzing C, *et al.* (2003). Identification and characterization of a nuclear interacting partner of anaplastic lymphoma kinase (NIPA). J Biol Chem 278, 30028–30036.
Ouyang W, Guo P, Takeda K, Fu Q, Fang H, Frucht DM (2020). ERK1/2 inactivation promotes a rapid redistribution of COP1 and degradation of COP1 substrates. Proc Natl Acad Sci USA 117, 4078–4087.
Palancade B, Zuccolo M, Loeillet S, Nicolas A, Doye V (2005). Pml39, a novel protein of the nuclear periphery required for nuclear retention of improper messenger ribonucleoparticles. Mol Biol Cell 16, 5258–5268.
Pédelacq J-D, Cabantous S, Tran T, Terwilliger TC, Waldo GS (2006). Engineering and characterization of a superfolder green fluorescent protein. Nat Biotechnol 24, 79–88.
Pérez-Garrastachu M, Arluzea J, Andrade R, Díez-Torre A, Urtizberea M, Silió M, Aréchaga J (2017). Nucleoporins redistribute inside the nucleus after cell cycle arrest induced by histone deacetylases inhibition. Nucleus 8, 515–533.
Raich N, Mahmoudi S, Emre D, Karess RE (2018). Mad1 influences interphase nucleoplasm organization and chromatin regulation in Drosophila. Open Biol 8, 180166.
Ran FA, Hsu PD, Lin C-Y, Gootenberg JS, Konermann S, Trevino AE, Scott DA, Inoue A, Matoba S, Zhang Y, *et al.* (2013a). Double nicking by RNA-guided CRISPR Cas9 for enhanced genome editing specificity. Cell 154, 1380–1389.
Ran FA, Hsu PD, Wright J, Agarwala V, Scott DA, Zhang F (2013b). Genome engineering using the CRISPR-Cas9 system. Nat Protoc 8, 2281–2308.
Reed SE, Staley EM, Mayginnes JP, Pintel DJ, Tullis GE (2006). Transfection of mammalian cells using linear polyethylenimine is a simple and effective means of producing recombinant adeno-associated virus vectors. J Virol Methods 138, 85–98.
Sabri N, Roth P, Xylourgidis N, Sadeghifar F, Adler J, Samakovlis C (2007). Distinct functions of the Drosophila NUP153 and NUP214 FG domains in nuclear protein transport. J Cell Biol 178, 557–565.
Schmid M, Arib G, Laemmli C, Nishikawa J, Durussel T, Laemmli UK (2006). Nup-PI: the nucleopore-promoter interaction of genes in yeast. Mol Cell 21, 379–391.
Schweizer N, Ferrás C, Kern DM, Logarinho E, Cheeseman IM, Maiato H (2013). Spindle assembly checkpoint robustness requires TPR-mediated regulation of MAD1/MAD2 proteostasis. J Cell Biol 203, 883–893.
Skaggs HS, Xing H, Wilkerson DC, Murphy LA, Hong Y, Mayhew CN, Sarge KD (2007). HSF1-TPR interaction facilitates export of stress-induced HSP70 mRNA. J Biol Chem 282, 33902–33907.
Snow CJ, Paschal BM (2014). Roles of the nucleoporin TPR in cancer and aging. Adv Exp Med Biol 773, 309–322.
Strambio-De-Castillia C, Niepel M, Rout MP (2010). The nuclear pore complex: bridging nuclear transport and gene regulation. Nat Rev Mol Cell Biol 11, 490–501.
Su Y, Pelz C, Huang T, Torkenczy K, Wang X, Cherry A, Daniel CJ, Liang J, Nan X, Dai M-S, *et al.* (2018). Post-translational modification localizes MYC to the nuclear pore basket to regulate a subset of target genes involved in cellular responses to environmental signals. Genes Dev 32, 1398–1419.
Tan-Wong SM, Wijayatilake HD, Proudfoot NJ (2009). Gene loops function to maintain transcriptional memory through interaction with the nuclear pore complex. Genes Dev 23, 2610–2624.
Texari L, Dieppois G, Vinciguerra P, Contreras MP, Groner A, Letourneau A, Stutz F (2013). The nuclear pore regulates GAL1 gene transcription by controlling the localization of the SUMO protease Ulp1. Mol Cell 51, 807–818.
Uhlířová J, Šebestová L, Fišer K, Sieger T, Fišerová J, Hozák P (2021). Nucleoporin TPR affects C2C12 myogenic differentiation via regulation of Myh4 expression. Cells 10, 1271.

Umlauf D, Bonnet J, Waharte F, Fournier M, Stierle M, Fischer B, Brino L, Devys D, Tora L (2013). The human TREX-2 complex is stably associated with the nuclear pore basket. J Cell Sci 126, 2656–2667.

Vaquerizas JM, Suyama R, Kind J, Miura K, Luscombe NM, Akhtar A (2010). Nuclear pore proteins NUP153 and megator define transcriptionally active regions in the Drosophila genome. PLoS Genet 6, e1000846.

Vollmer B, Lorenz M, Moreno-Andrés D, Bodenhöfer M, De Magistris P, Astrinidis SA, Schooley A, Flötenmeyer M, Leptihn S, Antonin W (2015). NUP153 recruits the NUP107-160 complex to the inner nuclear membrane for interphasic nuclear pore complex assembly. Dev Cell 33, 717–728.

von Klitzing C, Huss R, Illert AL, Fröschl A, Wötzel S, Peschel C, Bassermann F, Duyster J, von Klitzing C, Huss R, *et al*. (2011). APC/C(Cdh1)-mediated degradation of the F-box protein NIPA is regulated by its association with SKP1. PLoS One 6, e28998.

Walther TC, Fornerod M, Pickersgill H, Goldberg M, Allen TD, Mattaj IW (2001). The nucleoporin NUP153 is required for nuclear pore basket formation, nuclear pore complex anchoring and import of a subset of nuclear proteins. EMBO J 20, 5703–5714.

Wickramasinghe VO, Andrews R, Ellis P, Langford C, Gurdon JB, Stewart M, Venkitaraman AR, Laskey RA (2014). Selective nuclear export of specific classes of mRNA from mammalian nuclei is promoted by GANP. Nucleic Acids Res 42, 5059–5071.

Wu S, Chen K, Xu T, Ma K, Gao L, Fu C, Zhang W, Jing C, Ren C, Deng M, *et al*. (2021). Tpr deficiency disrupts erythroid maturation with impaired chromatin condensation in zebrafish embryogenesis. Front Cell Dev Biol 9, 1–16.

Yang Y, La H, Tang K, Miki D, Yang L, Wang B, Duan C-G, Nie W, Wang X, Wang S, *et al*. (2017). SAC3B, a central component of the mRNA export complex TREX-2, is required for prevention of epigenetic gene silencing in Arabidopsis. Nucleic Acids Res 45, 181–197.

Yi C, Li S, Wang J, Wei N, Deng XW (2006). Affinity purification reveals the association of WD40 protein constitutive photomorphogenic 1 with the hetero-oligomeric TCP-1 chaperonin complex in mammalian cells. Int J Biochem Cell Biol 38, 1076–1083.

Zhang P, Branson OE, Freitas MA, Parthun MR (2016). Identification of replication-dependent and replication-independent linker histone complexes: Tpr specifically promotes replication-dependent linker histone stability. BMC Biochem 17, 18.